CHALMERS

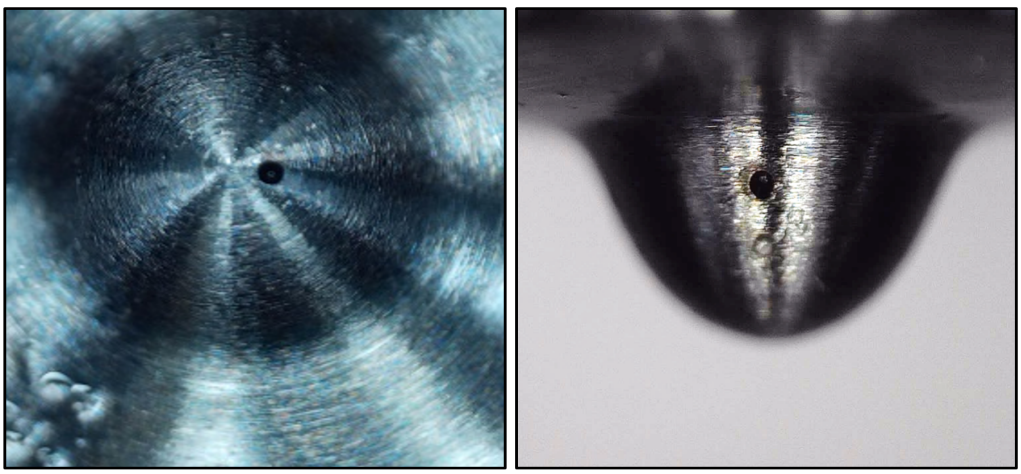

Measurement and evaluation of near-field spray kinematics

for nozzles with asymmetrical inlet geometries

MOHAMMAD NIKOUEI

Department of Mechanics and Maritime Sciences
CHALMERS UNIVERSITY OF TECHNOLOGY
Göteborg, Sweden 2022

THESIS FOR THE DEGREE OF LICENTIATE OF ENGINEERING IN THERMO AND FLUID DYNAMICS

Measurement and evaluation of near-field spray kinematics

for nozzles with asymmetrical inlet geometries

MOHAMMAD NIKOUEI

Department of Mechanics and Maritime Sciences

Division of Combustion and Propulsion Systems

CHALMERS UNIVERSITY OF TECHNOLOGY

Göteborg, Sweden 2022

Measurement and evaluation of near-field spray kinematics
for nozzles with asymmetrical inlet geometries
MOHAMMAD NIKOUEI

Thesis for the degree of Licentiate of Engineering 2022:01
ISSN 1652-8565
Department of Mechanics and Maritime Sciences
Division of Combustion and Propulsion Systems
Chalmers University of Technology
SE-412 96 Göteborg
Sweden
Telephone: +46 (0)31-772 1000

Cover:
Microscopic images of tested prototype nozzles: off-axis nozzle (left) and the two-hole nozzle (right).

Chalmers Reproservice
Göteborg, Sweden 2022

Measurement and evaluation of near-field spray kinematics
for nozzles with asymmetrical inlet geometries
MOHAMMAD NIKOUEI
Department of Mechanics and Maritime Sciences
Division of Combustion and Propulsion Systems
Chalmers University of Technology

Abstract

In diesel engines, fuel injection parameters have a commanding effect on mixing and combustion quality. This research aims to enhance the fundamental knowledge of fuel sprays and their primary break-up. In addition, this research provides statistical data to validate simulation models and improve the prediction accuracy in mixing and combustion.

This thesis report is based on evaluating the behavior and velocity profiles of near-field sprays generated by different inlet geometries under a range of injection pressures. The studied nozzles include single-hole nozzles with on-axis and off-axis orifices and a two-hole nozzle with angled orifices. We applied time-gated ballistic imaging to capture high-resolution spray images at the near-field. These high-resolution images provide a clear liquid/gas interface, which enables tracking of the spray structures. Furthermore, the displacement of the spray interface in two consecutive images over a specific time frame yields spray kinematics in two dimensions.

The results show how velocity measurements can describe spray development and evolution. Asymmetrical inlet geometries significantly affect near-field spray profile and targeting because the distribution of velocity magnitude on the two sides of the spray is not symmetric. In addition to inlet geometry, internal flow characteristics play a significant role in spray behavior. The outlook for this project mainly consists of the validation and development of simulation models. The obtained results provide an opportunity to correlate the near-field spray to the internal nozzle flow and study the effect of asymmetrical inlets on the internal flow.

Keywords: Diesel Spray, Ballistic Imaging, Nozzle Geometry, Spray Dynamics

List of publications

The thesis is based on the work contained in the following publications:

Publication A M. Nikouei and D. Sedarsky, *Near-field spray velocity and development in single-hole diesel injector*, 31st Annual Conference on Liquid Atomization and Spray Systems, Madison, WI, May 2021

Publication B M.Nikouei and D.Sedarsky, *Effect of asymmetrical orifice inlet geometry on spray kinematics and development*, submitted in *Fuel Journal Elsevier*

Acknowledgements

First, I would like to thank Per Stålhammar, Dennis Konstanzer, and Johan Linderyd from Scania CV AB for setting up this project and their supervision and support.

I want to thank my supervisor at the Chalmers University of Technology, David Sedarsky, who trusted me, and I appreciate him for his support, help, and guidance.

I want to say thank you to Lucien Koopmans and Mats Andersson, my co-supervisors, for their helpful and great advice for my research.

I could not run my experiments without receiving support from our lab engineers Patrik Wåhlin and Alf Magnusson. Anders Bragée also did an excellent job of fabricating the injector mount, and I am grateful to all of them.

Thanks to all staff and employees in the Combustion and Propulsion Systems division, especially Ammar Hazim Saber, whom I shared my office with. We had great discussions, and I learned a lot from him.

Finally, I have to thank my family, who supported me to reach this achievement.

Contents

1 Introduction

1.1 Motivation

According to studies, road transport has the largest share in transport of goods in Europe compared to water and rail transport, and we expect that this amount will increase more in the coming years [1]. Some sources estimate that CO_2 emissions of trucks and busses increase by 2.2% every year, which is largely due to the increase in transportation volume [2]. CO_2 and NO_x are the main pollutant emissions from heavy-duty vehicles and harm public health and the environment. Therefore, it is highly desirable to reduce emissions of such vehicles to near-zero value and replace them with older technologies [3].

In Compression Ignition (CI) engines, fresh air is drawn into the cylinder and compressed by piston movement. This compression increases the gas temperature. When fuel is injected into this hot air, the resulting combustion reaction increases the pressure inside the combustion chamber and pushes the piston down. In diesel engines, the fuel is injected at extremely high pressure through relatively small nozzle holes. When the high-pressure flow exits the nozzle orifices, the injected fuel turns into droplets and mixes with the surrounding gas. This mixing process can significantly affect combustion quality and its products [4]. Accordingly, the fuel injection characteristics have a crucial effect on the mixing and combustion quality [5, 6]. Therefore, we can expect to enhance engine efficiency and minimize pollutant emissions by controlling the fuel injection properties in a particular configuration. However, it is challenging to find the optimum fuel injection characteristics due to the presence of many parameters involved in the spray formation and mixing process, such as nozzle geometry, injection pressure, ambient pressure,temperature, gas density, and fuel properties. These parameters directly influence fuel spray characteristics, and there are interactions between them. In addition, the engine operates at various load and speed conditions so that some of the injection parameters, such as injection pressure and injection rate, are not constant. Nozzle geometry also plays a significant role among these parameters since it is responsible for distributing and targeting fuel droplets. Numerous studies confirm that nozzle geometry can directly impact mixing and combustion characteristics [7, 8, 9]. However, nozzle geometry is defined by various parameters such as orifice diameter, conicity, cross-sectional shape, orifice length, number of orifices, and orifice angle, making it more complicated to find the best nozzle design for specific applications.

1.2 Objectives

In order to achieve sustainable development goals, we have to speed up the development of vehicle powertrains, especially with regard to emission reduction. For this purpose, a

promising approach is to implement simulation models to find the most optimum design for processes involved in an engine, including the fuel injection. A number of simulation models can predict these processes to a relatively high accuracy levels; however, they require high computing power and, therefore, high financial and time costs. In order to reduce these costs, we need to develop simpler models, which must be evaluated and validated based on experimental data.

Flow in the nozzle sac volume and near-field dominate fuel spray formation. These flows are responsible for fuel distribution and temporal evolution of the in-cylinder mixing conditions. Therefore, the main objective of this study is to measure spray kinematics to establish fundamental knowledge for spray break-up and understand how inlet geometry influences spray behavior at various operating conditions. In addition, this will provide input to validate Computational Fluid Dynamics (CFD) models. Therefore, this research can also indirectly contribute to improving mixing and combustion quality prediction. For this purpose, the main focus of this research is on measurements of near-field spray velocity with on-axis, off-axis, and two-hole geometries to study how the interior and near-nozzle flows affect spray morphology.

2 Fundamentals

2.1 Diesel combustion

Diesel fuel contains long-chain hydrocarbon molecules that ignite rapidly in the presence of high-pressure and high-temperature air. The role of the fuel injection system in the diesel engine is metering and delivering a desired amount of fuel to the combustion chamber at a certain crank angle. In addition, the fuel must be distributed in the combustion chamber for efficient mixing with compressed air.

Diesel combustion is mixing controlled; in other words, the heat release rate is a function of the efficiency with which fuel droplets are evaporated and mixed with air. In addition, the amount of injected fuel controls the speed and torque in CI engines. The combustion process of Diesel fuel is somewhat complex because it consists of turbulent and three-dimensional reactions that occur in a high-temperature and high-pressure environment. Therefore, detailed measurements of the events within a reacting diesel fuel jet have always been challenging. However, the advent of advanced laser diagnostics significantly improved the knowledge about fuel sprays [10].

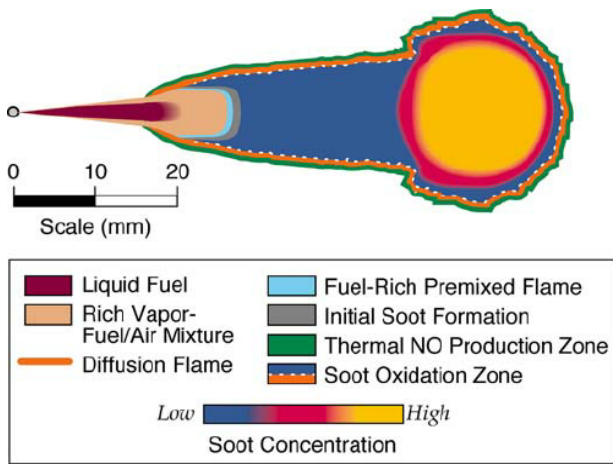

Figure 2.1: *Conceptual model for diesel combustion by J.D. Dec [10]*

Unlike Spark Ignition (SI) engines, CI engines do not have special air/fuel ratio requirements. Diesel engines operate with heterogeneous mixture formation and auto-ignition, thus making it challenging to achieve an entirely homogeneous air-fuel mixture prior to or during the combustion. Therefore, the mixture encountered in a diesel engine includes a range from $\lambda = 0$ (pure fuel) at the near-field spray to $\lambda = \infty$ (pure air) at the outer extremities of the spray jet. The excess-air factor (λ) indicates the ratio of available air to required air mass for stoichiometric combustion [11]. In addition, CI

engines produce much less unburned hydrocarbon (HC) and carbon monoxide (CO) due to the abundance of oxygen in the combustion chamber. However, CI engines produce more particulate matter and nitrogen oxides (NOx). Dec model [10] can explain the pollutant formation process in diesel combustion. According to this model, soot is primarily formed in the fuel-rich mixing zone, while NOx is formed in the hotter reaction zones at the edge of the fuel plume. Accordingly, the soot formation and burning rate largely depend on the amount of fuel mixed with air and the equivalence ratio. On the other hand, NOx is more likely to form on the outer surface, where the fuel-air mixture is lean. Therefore, it is necessary to establish a trade-off between soot and NOx formation, which requires an optimal control of fuel-air mixing.

2.2 Spray

The conversion of liquid flow to the form of tiny droplets is called spray. In combustion engines, the fuel is injected in the form of a spray to promote the distribution and mixing of the fuel with air. In general, spray formation is divided into primary and secondary break-up sections. Once the flow exits the nozzle orifice, a combined effect of turbulence, cavitation, and aerodynamics forces transform the flow into ligaments and large droplets, often termed primary break-up. The secondary break-up is the process in which these large droplets break into smaller ones, and aerodynamic forces dominate this process in fuel injection sprays.

2.2.1 Instabilities

Turbulence and cavitation are the main disturbances in the internal nozzle flow. Turbulence is generated by interactions between high-speed flow and surrounding walls, and it has a strong effect on primary breakup and surface wake growth. The role of cavitation on atomization is less clear, but its transient behavior and interactions with exit velocity and pressure fluctuations certainly contribute to primary breakup. Reynolds (Re) number (equation2.1) can estimate the turbulence level in a flow, and a higher Reynolds number means higher turbulence intensity. Reynolds number is defined as the ratio of inertial forces to viscous forces within a fluid,

$$Re = \frac{\rho.\nu.d}{\mu}, \tag{2.1}$$

where ρ is the fluid density, ν is flow velocity, d is the channel cross-sectional area, but it will be equal to orifice area in the case of fuel injection, and μ is the fluid (fuel) viscosity.

The breakup of a droplet in a jet flow is governed by dynamic pressure, surface tension,

and viscous forces. In most cases, the ratio of the aerodynamic forces and the surface tension forces determine the deformation of a drop. The ratio of these two opposing forces is the Weber (We) number (equation 2.2). The higher the Weber number, the more significantly the deforming pressure forces are compared with the reforming surface tension forces. In addition, a particular range of Weber numbers dictates specific breakup mechanisms, as depicted in Figure2.3.

$$We = \frac{\rho.\nu^2.d}{\sigma}, \tag{2.2}$$

where ρ is the fluid density, ν is flow velocity, d is the flow cross-sectional area, and μ is the fluid viscosity.

According to Reitz [12], four regimes of breakup are encountered as the liquid injection velocity is progressively increased. Figure 2.2 indicates in these regimes, including Rayleigh mechanism, first wind-induced, second wind-induced, and atomization regimes. The diameter of the produced droplets characterizes these regimes. In addition, the diagram shows that the jet instabilities can be characterized by Ohnesorge (Oh) and Reynolds numbers. The Ohnesorge number (Oh) relates the viscous forces to inertial and surface tension forces and can be written as equation **??**.

Among the defined jet break-up regimes, the fuel injection in diesel engines is classified as the atomization break-up regime. The atomization regime occurs with extreme jet velocities. Aerodynamic interactions at the liquid/gas interface appear to be one major component of the atomization mechanism in this regime, producing droplets whose average diameter D is much smaller than the nozzle diameter. Since the fuel jet atomizes into droplets of different dimensions, a mean diameter has to be defined to characterize the break-up quality. For this purpose, the so-called Sauter Mean Diameter (SMD) is used. The SMD is defined as the diameter of a droplet with the same volume/surface area ratio of the fuel jet. The atomization and evaporation of fuel improve if SMD decreases because the required time for evaporating a spherical droplet is proportional to the droplet diameter. This improvement can be achieved by smaller nozzle diameter, higher injection pressures, lower fuel viscosity, and surface tension.

The quality of the break-up can be classified by non-dimensional numbers such as Reynolds (equation2.1), Ohnesorge (equation 2.3) and Weber (equation 2.2). [13, 14].

$$Oh = \frac{\mu}{\sqrt{\rho.\sigma.d}} \tag{2.3}$$

Similarly, different regimes have been observed for the secondary break-up, as shown in Figure 2.3. As mentioned earlier, aerodynamics force is the main mechanism involved in this process. Therefore, Weber number, which is the ratio between dynamic pressure to the surface tension, can determine the characteristics of this break-up process.

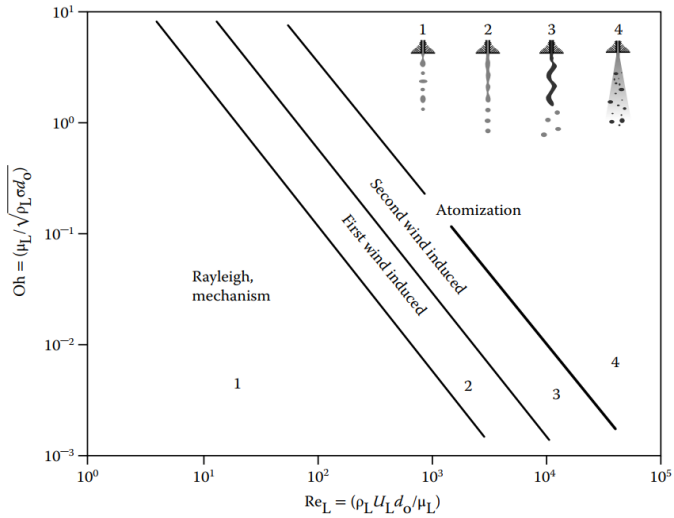

Figure 2.2: *Primary break-up diagram [15]*

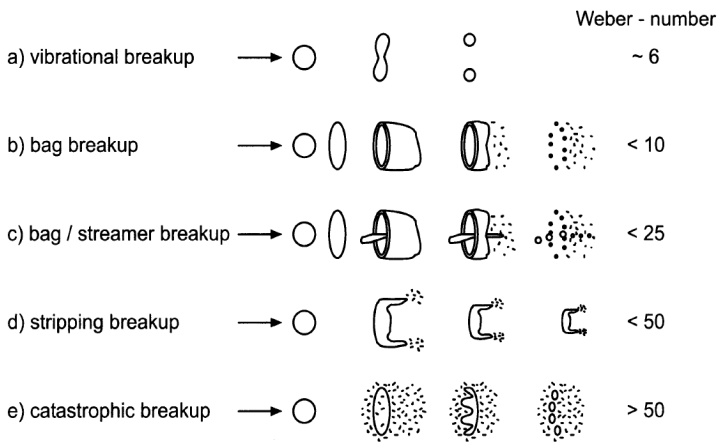

Figure 2.3: *Secondary break-up mechanisms classified by Weber number [13]*

According to equations 2.1, 2.2, and 2.3, it is apparent that flow velocity, density, and the surface tension of the fuel play an essential role in the quality of the break-up. It is worth noting that nozzle geometry also contributes to creating turbulence and cavitation, which affects the break-up and atomization.

2.2.2 Spray velocity

The flow characteristics at the nozzle exit are generally governed by the flow state upstream of the orifice and disturbances generated in the nozzle. For a given nozzle, the geometry parameters are constant, so the nature of the flow (laminar or turbulent) is dictated by the Reynolds number and velocity. In other words, there are links between nozzle geometry, the internal flow characteristics, and the near-field spray dynamics that affect break-up characteristics. For instance, if the flow at the orifice is fully turbulent, the radial velocity component leads to disruption of the surface film, followed by a general disintegration of the jet. In the case of fully turbulent flow, no aerodynamic forces are required for the break-up. Even when injected into a vacuum, the jet will disintegrate solely under the influence of turbulence [15, 16].

As soon as the flow leaves the nozzle and the physical constraint of the nozzle wall is removed, the velocity profile relaxation occurs by a mechanism of momentum transfer between transverse layers within the jet flow. This change in velocity profile that occurs downstream of the nozzle exit can influence the stability of the jet and its subsequent break-up into drops [15, 17]. Therefore, the internal motions associated with profile relaxation create another disruptive mechanism in addition to the jet-destabilizing forces discussed earlier.

2.2.3 Cavitation

When the local pressure in a liquid stream drops below the fluid's vapor pressure, vapor bubbles are formed, and this phenomenon is called cavitation. Cavitation usually occurs in applications involving high pressure gradients such as pump impellers, marine propellers, and fuel injectors. The vapor bubbles will collapse quickly upon their formation; the explosion of bubbles will induce high pressures on the contact surfaces, which has a destructive effect on surfaces in the long term. Although cavitation can be harmful to the nozzle hole structure, it can enhance atomization and prevent deposits from forming in the nozzle [18].

Inside the injector nozzle, the fuel flows at high pressures, and this flow exits from tiny orifice holes. When the fuel comes in contact with the relatively sharp edges at the orifice inlet, a separation of the boundary layer from the orifice wall occurs, and it creates so-called "vena contracta" (Figure 2.4), which includes a recirculation zone [19]. As Figure 2.4 illustrates, the cross-sectional area becomes smaller. In addition, the velocity of the flow increases as a consequence of the reduction in friction between flow and internal orifice wall. Accordingly, the acceleration of flow causes pressure depression. If the pressure drop is significant enough, cavitation occurs, and vapor bubbles appear. In general, as the edge radius gets smaller, the probability of cavitation occurrence becomes more significant [20].

Several factors can affect the cavitation intensity, such as the pressure difference.

Accordingly, as the pressure difference between the mass flow rate and the average velocity increases, the discharge coefficient does not change much [21].

2.3 Injection system

High injection pressure and fast responsive injectors with variable discharge rates are desirable for increasing the efficiency and controllability of diesel engines. The common-rail system can vary injection timing and pressure over wide ranges. In this system, a rail accumulates fuel at high pressure, and injectors are connected to the rail by short pipes. The injectors are triggered and controlled by electrical signals and integrate the injection control valve and the atomizing nozzle. Thus injector and the nozzle unit are the key elements in this system [22].

2.3.1 Injector

In common-rail injection systems, the combination of injector needle dynamics and nozzle geometry specifies the quantity of the injected fuel and the structure of the diesel spray. Needle actuation and the transient hydraulics from the rail to the nozzle tip govern injection dynamics. The needle actuation is usually done in two general ways including solenoid-valve and piezo actuator.

Figure 2.5(a) depicts the operation modes of the solenoid-valve injector. In this configuration, all cavities, including the control chamber, are filled with high-pressure fuel and create a positive pressure at the top of the needle to keep it close. As soon as the solenoid coil is excited by an electrical signal, the solenoid armature moves upward, causing fuel flow from the valve control chamber to the cavity and the fuel tank through the return line. However, the inlet restrictor prevents a complete pressure compensation; thus, the valve-control chamber pressure falls below the nozzle chamber pressure. Therefore,

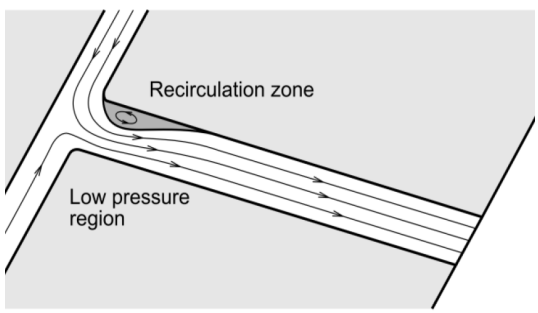

Figure 2.4: *A simplified sketch of cavitation and vena contracta occuring in the nozzle hole [19].*

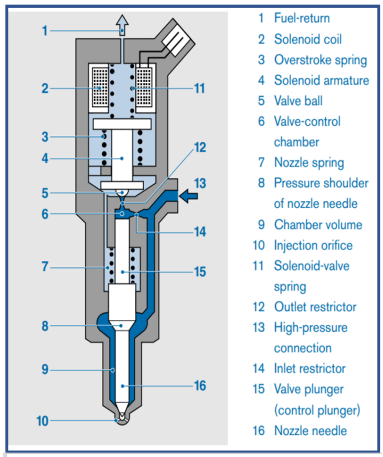

(a) Solenoid

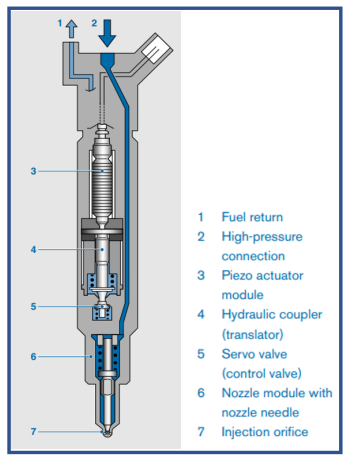

(b) Piezo

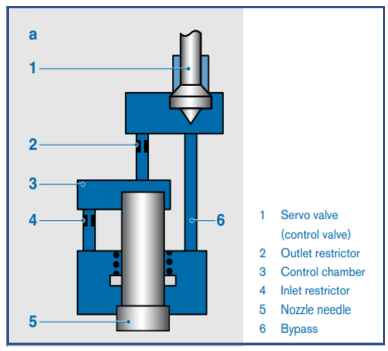

(c) Control-valve

Figure 2.5: *Common mechanisms for injector needle actuation (adopted from [23])*

the force acts on the control plunger and opens the nozzle needle. In order to stop the injection, the solenoid triggering signal is switched off. As a result, the valve spring presses the armature down, and the valve ball closes the outlet restrictor. Thus, pressure in the control chamber rises again and results in a greater force on the control plunger. The force on the valve-control chamber and the nozzle-spring force exceeds the force acting on the nozzle needle, closing the nozzle needle.

The piezo actuator injectors enhances the injector stability and drift compared to solenoid systems because no mechanical force acts directly on the needle. In addition, this design reduces the moving masses and friction. It also provides a fast-responding injector with the capability of very short intervals between injection events. The working principle of this injector is similar to the solenoid-valve injector. However, the main

difference between these two configurations is the control valve operation in the Piezo injector. Fig 2.5(b) illustrates the operation of the control valve. The rail pressure in the control chamber keeps the nozzle closed. When the piezo actuator is triggered, the servo valve opens and closes the bypass passage. The flow-rate ratio between the outlet and the inlet restrictors lowers the pressure in the control chamber, resulting in nozzle opening. The control volume flows via the servo valve to the low-pressure circuit of the overall system. For closing the nozzle, the servo valve releases the bypass passage. Thus, the inlet and outlet restrictors reverse and refill the control chamber to raise its pressure. As soon as the required pressure is attained, the nozzle needle starts to move, and the injection process ends.

The injectors used for this research are of XPI (eXtra high Pressure Injection) type, developed by Cummins. These injectors are capable of injection pressures up to 2400 bar. Fuel enters the cavity into the injector body from the side of the injector through the High Pressure Connector (HPC). A typical XPI injector has three main modules: stator, control, and nozzle (Figure 2.6). The stator has a electromagnetic winding, and by receiving an electrical signal, it pushes the armature plate upward. The plunger movement creates a flow through the control valve, causing a pressure depression in the control chamber. Therefore, the needle moves upwards due to the high-pressure gradients on both ends. Consequently, the sac volume is filled with fuel which flows out through the nozzle holes, and injection begins. The springs push the plungers down and stop the flow as soon as the electrical signal turns off.

2.3.2 Nozzle

A typical injector has a nozzle with 8 to 12 holes (orifices) to distribute the fuel into the combustion chamber. Nozzle orifices can exist in various geometrical configurations. The main parameters that describe the orifice geometry include conicity, length to diameter ratio (L/D), orifice angle, and orifice position. Figure 2.7 depicts some of these parameters. In addition, k-factor is a parameter used to describe the conicity level of the orifice (equation 2.4). In this equation D_i and D_o are the inlet and the outlet diameters, respectively, and L is the length of the orifice.

$$k_f = \frac{D_i - D_o}{10L} \tag{2.4}$$

The nozzle design affects internal flow, which potentially influences the spray characteristics. As an example, Figure 2.8 shows the flow pattern inside the sac volume and the orifice inlet. This figure shows that the flow pattern on the sides of the orifice inlet is not symmetrical and the flow must make sharper turns and detours on one side. It is expected that asymmetrical flow patterns generate more turbulence and cavitation, and consequently impact spray characteristics.

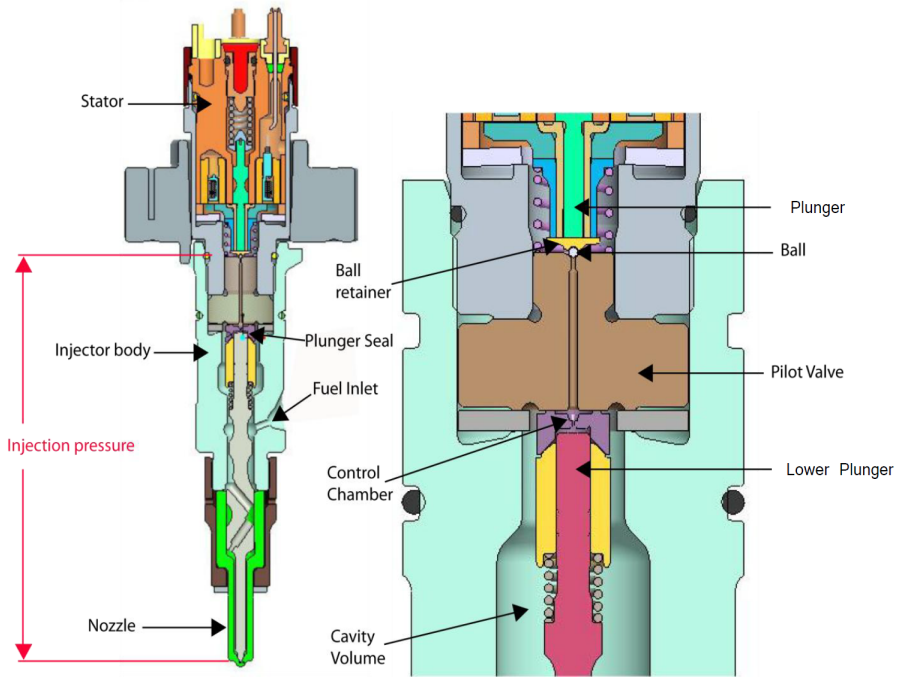

Figure 2.6: *a half-section layout of an XPI injector and its main components.*

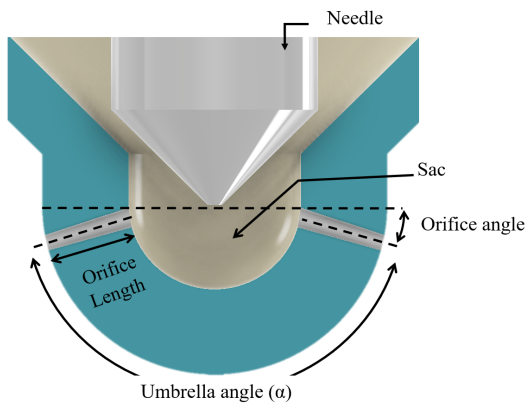

Figure 2.7: *A typical injector nozzle and its geometrical parameters*

2.3.2.1 Nozzle geometry and spray characteristics

Nozzle geometry can play an essential role in cavitation and its intensity. The roughness of the orifice wall, sharpness of the orifice inlet edge, length/diameter ratio, orifice angle, and conicity are among the most influential geometry parameters regarding cavitation.

An analysis [24] shows that orifice inclination angle influences cavitation intensity. In general, as the umbrella angle (α) increases, cavitation is more likely to occur, and its intensity will be higher. In addition, a larger umbrella angle decreases mass flow rate and momentum flux due to the higher deflection in streamline while the velocity of the flow increases. The inclination angle also determines the roundness of the orifice inlet edge.

The number of nozzle orifices affects both the fuel distribution and the behavior of individual spray. For example, comparing a single-hole with a multi-hole nozzle [25] indicates that at the same rail pressure, nozzle sac pressure re-builds faster in the single-hole case. At the same time, there is a higher fluctuation in sac pressure for the multi-hole nozzle. As a result, spray angle will be higher in multi-hole nozzle while spray penetration is lower than in the single-hole case. This fluctuation is mainly due to eccentric needle motion and causes hole-to-hole spray variations [26]. In addition, fluctuations in spray dynamics are more significant in the transient phase but the stabilized.

The air entrainment velocity depends on the spray cone angle. The larger cone angle enhances the air-fuel mixing, especially in transient phases [27]. Nozzle geometry and ambient density are the main parameters that affecting spray cone angle [28, 29] while injection pressure has negligible effect on that [30, 31]. Often the spray angle is inversely related to the spray penetration length; i.e., a wider spray has a shorter penetration length at the same injection rate [29, 28].

A convergent orifice (k-factor>0) provides a higher mass flow rate and discharge coefficient with less cavitation intensity compared to the divergent orifice (k-factor < 0) [21]. In addition, a large k-factor generates a smaller spray cone angle and Sauter Mean Diameter (SMD) while accelerating spray tip penetration evolution [32].

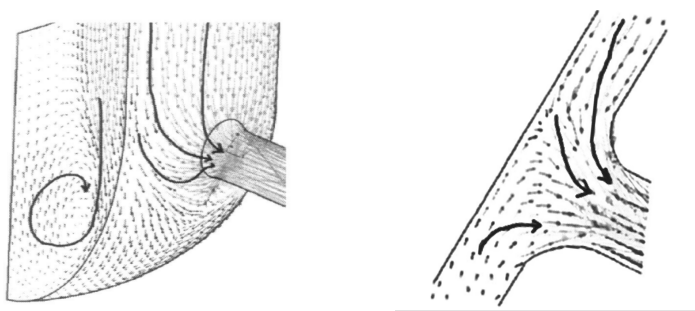

(a) (b)

Figure 2.8: *A schematics example of flow streamlines a) inside a large sac volume, b) at the orifice entrance. (adopted from [33])*

2.3.2.2 Hole-to-hole variation

The sac volume functions as a buffer, producing a more consistent flow distribution among the spray holes. It also produces a smoother transition and a more streamlined entrance into the metering holes. However, at the end of the injection, still, a considerable amount of fuel trapped in the sac volume and may exit the nozzle orifice at low injection pressure. Therefore, a large sac volume may create more soot and unburnt hydrocarbons [33]. In some cases, the holes are created at the needle seat instead of the sac volume. This can reduce soot formation at the end of the injection but it creates significant hole-to-hole variations.

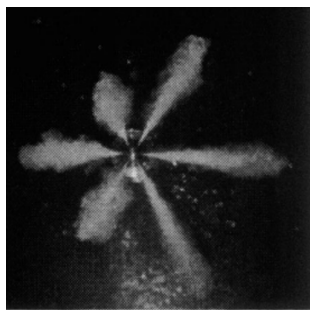

Figure 2.9: *hole-to-hole variation and unequal sprays*

Hole-to-hole variations may have other reasons as well, that are divided into three main categories:

1. Geometrical differences in orifices are the main reason, which can be the result of poor manufacturing quality, erosive damage, or variable amounts of coke deposition.

2. Installing the injector with an inclination angle generates orifices with different angles with the horizontal plane. Thus, the flow path for those orifices will differ, resulting in hole-to-hole spray variations.

3. The eccentric needle motion affects the internal flow and induces oscillations in spray velocity. However, studies show that for a multi-hole injector, the oscillation phase, frequency, and amplitude of spray axial velocity are similar for all holes regardless of the number of holes. In addition, the needle lift also influences the internal flow and hole-to-hole spray variations. The needle seat area is smaller than the hole area for small lift; Therefore, a slight needle mismatch contributes to the misdistribution of the needle seat area (incoming flow area) and internal flow. However, as the needle lift, and thus, the needle seat area increases, this effect becomes more negligible. The internal flow area determines the flow state and spray characteristics behavior. The internal flow area determines the flow state and thus injected spray characteristics; the moment the needle seat area is equal to the nozzle hole area is understood as the turning point from transient flow to

quasi-steady state flow. Therefore, the effect of needle mismatch on hole-to-hole variations appears mainly during the opening and closing of the needle and not for the fully developed flow.[34].

3 Method

This work investigates the effect of the nozzle geometry on the near-field spray kinematics. For this purpose, we measure the velocity of the near-field spray formed by three nozzles with specific geometries under different injection pressures. The approach applies time-gated ballistic imaging to produce double-frame and time-resolved images with high resolution. With the aid of a normalized cross-correction algorithm, spatial structures on the spray interface are detected and tracked in each pair of images. The relative displacement of fluid structures of the spray over the time frame between two images is the approximate velocity of that area of the spray.

3.1 Nozzle geometries

This study contains an experimental investigation of four prototype nozzles and measurements of their spray kinematics. Figure 3.1 illustrates schematics of these nozzles, and Table 3.1 provides nozzles specifications. As can be seen, the first two nozzles (SH1 and SH2) are both single-hole, and their orifice axis is aligned with the injector axis. Therefore, both orifices have a relatively symmetrical geometry along their axes (Figures 3.1(a) and 3.1(b)). The only differences between the two nozzles are the orifice diameter and k-factor. Although the third nozzle (OA) is also a single-hole nozzle, its orifice axis is located parallel to the injector with a short distance from the centerline. Therefore, it has an asymmetric geometry at the inlet and outlet of the orifice (Figure 3.1(c)). Unlike the other nozzles, last one (TH) has two orifices with umbrella angle of 146°(Figure 3.1(d)). Regarding the geometrical aspects, this nozzle is very similar to the nozzles currently used in production, but it is more practical to study a simplified geometry with fewer holes. This nozzle allows investigating hole-to-hole spray variations while oblique orifices also create asymmetrical geometry.

Table 3.1: Nozzles specifications

Nozzle	$SH1$	$SH2$	OA	TH
Number of orifices	1	1	1	2
Nominal outlet diameter [μm]	140	180	220	200
k-factor	0	2	1.4	2
Hydro-grinding level [%]	30	30	15	15
Spray target angle [°]	90	90	90	17

3.2 Velocity measurement

The most common method for measuring flow velocity is the Particle Image Velocimetry (PIV) method. In this method, seeding particles are added to the flow, and two successive laser sheets illuminate them to create double frame images. The measurement of relative displacement of these particles yields the flow's local velocity. It is done by applying cross-correlation in two consecutive images over a specified time frame. Although this method has proved high accuracy, it is not practical for near-field spray application due to high flow density. In this spray region, either no particle is formed, or they are too small to be detected. In other words, this method is applicable for more dilute spray regions. Therefore, in this research work, the cross-correlation is applied to the fluid interface structures instead of using seeding particles. However, in order to accurately detect and track these structures, it requires high image resolution and minimizing optical noise. Among the various methods available for spray imaging, the Ballistic Imaging (BI) method can produce images with such desired properties. For the first time, Sedarsky et al. [35] successfully obtained near-field spray velocity vectors using this method. However, velocity measurements for the current application are limited to the spray periphery only, because the the flow is too dense at the spray core. Therefore, this method cannot provide data of the liquid core velocity at the current stage. However, applying the same measurement procedure on different spatial planes at different view angles (rotated around the orifice axis) makes it possible to understand overall spray behavior and its velocity profile. Similarly, Sedarsky et al. have proven the applicability of this approach [36].

3.3 Optical setup

Time gated ballistic imaging is a line-of-sight imaging method that was initially used for medical purposes, but this method was performed to study sprays after a while. The principles of this method are described in detail by Linne et al. [37]. In short, the photons passing through the spray without colliding with the spray or with little impact have a higher speed than the others, and they reach the detector faster. In addition, a so-called optical shutter rejects the multi-scattered photons and allows the other photons to reach the camera to record high-resolution spray images. This optical shutter is called the OKE gate and consists of two cross-polarizers and a birefringence medium. When a switching pulse activates birefringence in that medium, the polarization of transmitted photons rotates by 90°, and photons can go through the second polarizer. However, the gate activation period is approximately 2 ps; therefore, any photon that reaches the medium after the activated period cannot find a way through the second polarizer. Consequently, this imaging method can eliminate noises coming from multiple scattering to reduce image blurring and create sharp images with high resolution.

Ballistic images are two-dimensional representations of three-dimensional structures, and they can show large features that refract light instead of scattering small droplets.

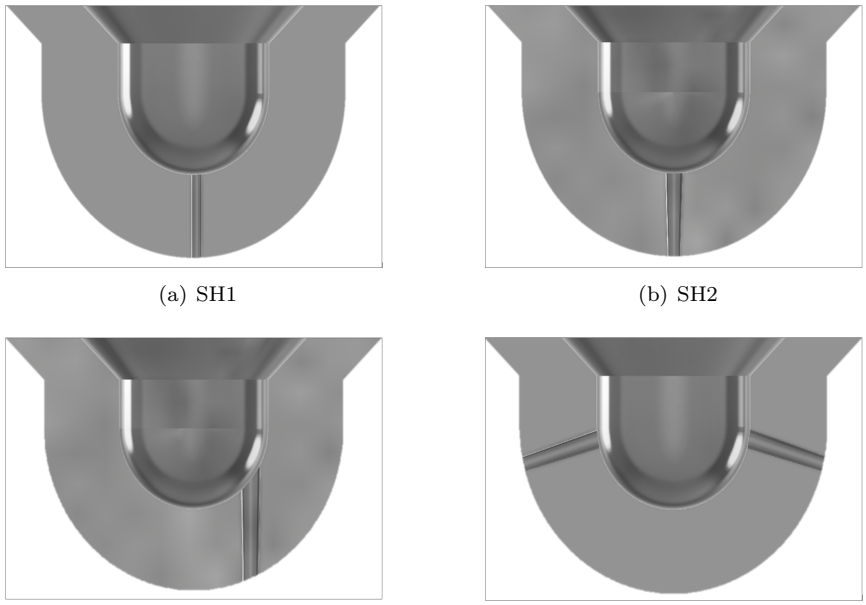

(a) SH1 (b) SH2

(c) OA (d) TH

Figure 3.1: *Half-section view of the nozzle geometries.*

However, The liquid volume fraction of these structures might be smaller than 100% because they could consist of distributed sheets with entrained gas [38]. Nevertheless, the images appear monolithic even if the interior consists of a mixture. The utility of BI is to reveal the left and right-hand edges of liquid structures buried inside drop clouds. As Falgout et al. [39] have shown earlier, The spray structures in ballistic images are distinct and provide a well-defined interface. In contrast, these edges are diffuse in shadow images with structures that indicate a dropping cloud (Figure 3.3). Therefore, there is no clear, defined gas/liquid interface, as seen in the BI of the same jet.

The optical arrangement for imaging system is according to the "collinear ballistic imaging" [40]. In this configuration, the frequency of the imaging beam differentiates from switching pulse, and both of them reach the OKE gate in a co-linear configuration. The optical setup for this work is based on collinear ballistic imaging with two lenses (4 focal points) as depicted in Figure 3.2. In this setup, two 100 fs laser pulses with the wavelength of 800 nm are generated with an adjustable time difference. First, both beams are aligned together using a beam-splitter. Then, a beam-splitter divides each beam into two portions; the part containing higher energy works as the switching beam after being transmitted through the delay stage. Finally, the other portion will be transmitted through the spray and camera to construct the spray image. A double-frame ICCD camera records the image signals.

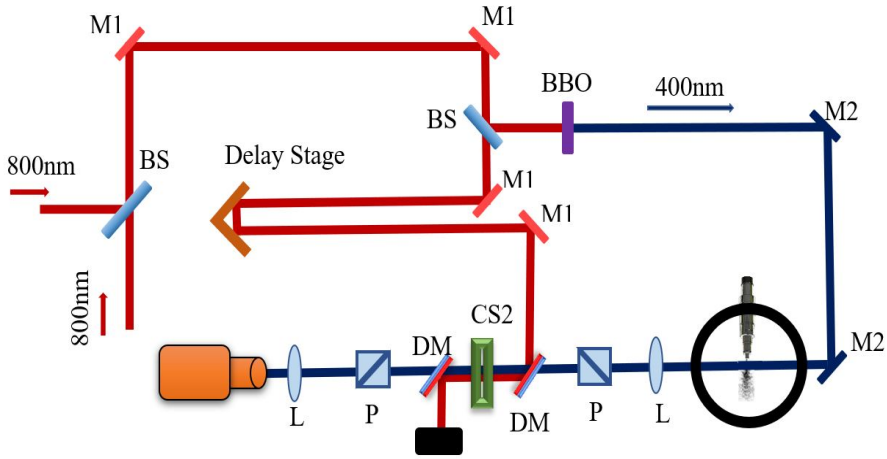

Figure 3.2: *A schematic view of image acquisition system configuration. M1: 800 nm mirror, M2: 400 nm mirror, BS: beam splitter, P: polarizer, L: lens, DM: dichroich mirror.*

This configuration allows recording only one image per laser pulse for each injection event but that provides more information about the spray structure and preserves spray interface in high resolution. Therefore, recording the entire injection process is unattainable, as is usually done by high-speed video cameras. Hence, the approach to this problem is to perform statistical velocity measurements. In this approach, we first perform image acquisition for discrete-time instants from the start of injection to 50 μs. We should take between 150 and 200 images for each step to provide a sufficient statistical population to measure the statistical velocity.

3.4 Design of experiment

The experiments were performed at the spray laboratory at Chalmers university of technology. In these experiments, fuel injections occur into a chamber operating at atmospheric conditions. A high-pressure pump supplies fuel to the injector over a range of pressures up to 1600 bar. We have set three levels of low, medium, and high injection pressures for the experiments. Table 3.2 displays other experimental conditions.

Here, the Start Of Injection (SOI) refers to the moment that spray is on the verge of leaving the nozzle, and other time-instants are relative to this moment. In order to determine the SOI, a set of images is taken just before the estimated SOI until the flow becomes visible. We set the time increment between images to 1 μs. Assuming that

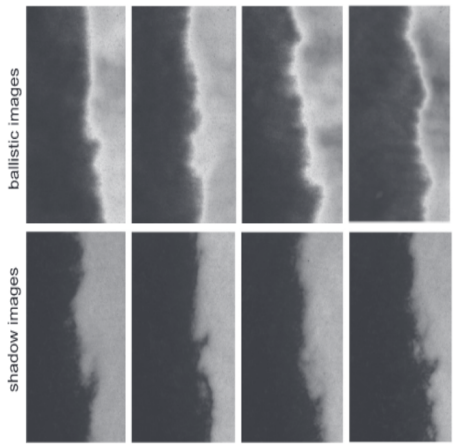

Figure 3.3: *Comparison between ballistic images (top) and shadow images (bottom) [39]. It shows that ballistic images provide a more clear liquid/gas interface than the shadow images of the same nozzle and fuel.*

Table 3.2: Experimental conditions

Parameter	**Value**	**Unit**
Rail pressure	800, 1200, 1600	*bar*
Back pressure	atm	-
Ambient temperature	294	*K*
Injection duration	2	*ms*
Image pairs time difference	560	*ns*

the velocity of the spray at the beginning of injection is linear, measuring the average displacement of the spray leading edge makes it possible to calculate the hydraulic SOI time instant.

3.5 Data processing

Image processing procedures apply to all images, including background removal and normalizing. In addition, bilateral filters are applied to minimize the noise due to the non-uniformity of the laser beams or to filter residual from previous injections. Implementing a region-matching algorithm, one can extract velocity vectors. This algorithm is described in detail in [35] and [41]. As a short explanation, we define a set of windows called "template" and "search field" and adjust their size according to the application. Then, the Sobel edge detection method catches the spray periphery, and several points are distributed on the edge of the spray as "target points". Each target point is the origin of

a template window. The texture and intensity information inside the template should match with a window in the search field area in the second image. The position difference of those template origins windows yields a displacement vector in 2 dimensions for each target point. Finally, each vector can be validated or rejected based on the user input parameters, such as allowable displacement or cross-correlation coefficient.

It is worth mentioning that all images taken at any time instant indicate the diversity of the spray profiles. Therefore, we can construct an overall spray profile by calculating the average of all the images at the respective time step. Then, by averaging all available velocity data in the vicinity of any point on the overall spray profile, the average velocity for each point is calculated as the local velocity.

4 Results and discussion

This section presents a summary of the results presented in the appended articles. Figures 4.1 and 4.2 illustrate velocity profiles for the periphery of the near-field spray at discrete time instants after the start of injection. Each figure contains velocity information and the spray profile for five orifices at different injection pressures. We have rotated or flipped the spray profiles horizontally for the off-axis (OA) and two-hole nozzle (TH) so that the side with a sharper inlet edge lies on the negative side of the horizontal axis.

4.1 General trends

The results consist of the velocity data in the transient phase of the early injection. In this phase, the nozzle opening delay and the needle position also affect the flow velocity. For instance, by comparing the injection pressure, it is apparent that the spray profile and its velocity are different at the corresponding time steps for measurements at different pressures. Nevertheless, a comparison between spray profiles of the OA nozzle reveals that the spray profile at 30 μs after SOI under 1600 bar is similar to the spray at 800 bar and 40 μs. However, instantaneous local velocities are generally higher at 1600 bar.

Shortly after leaving the nozzle, the fuel is accelerated, and a mushroom-shaped mass forms. The root of this mass seems to be related to the residual fuel trapped in the nozzle's sac volume from the previous injection. This mass is pushed down by the pressure of the fluid coming out of the nozzle. Since the cross-sectional area of this mass is large, the drag force on the flow becomes more significant and it induces deceleration to the flow. Nevertheless, The incoming high-pressure fuel recovers the spray velocity. Finally, the velocity profile becomes more stable at the quasi-steady state (800 μs after SOI).

4.2 Effect of nozzle geometry

Each row of Figures 4.1 and 4.2 consist of velocity profiles of a specific nozzle at different time steps. The comparison of these rows indicates that the overall spray velocities for both orifices of the two-hole nozzle are considerably lower than the off-axis nozzle. The difference in the total discharge cross-sectional area and the needle position could be the potential reason for that. Since the needle position is low at the beginning of the injection, the ratio between the incoming and outgoing flow rate in the sac volume is low. In addition, the presence of two orifices increases the discharge area and outgoing flow rate, which leads to an even lower sac inlet/outlet discharge rate, and it causes a longer time for sac pressure recovery. When the needle reaches the highest lift position (at the quasi-steady state), the differences between overall spray velocities for the off-axis and the

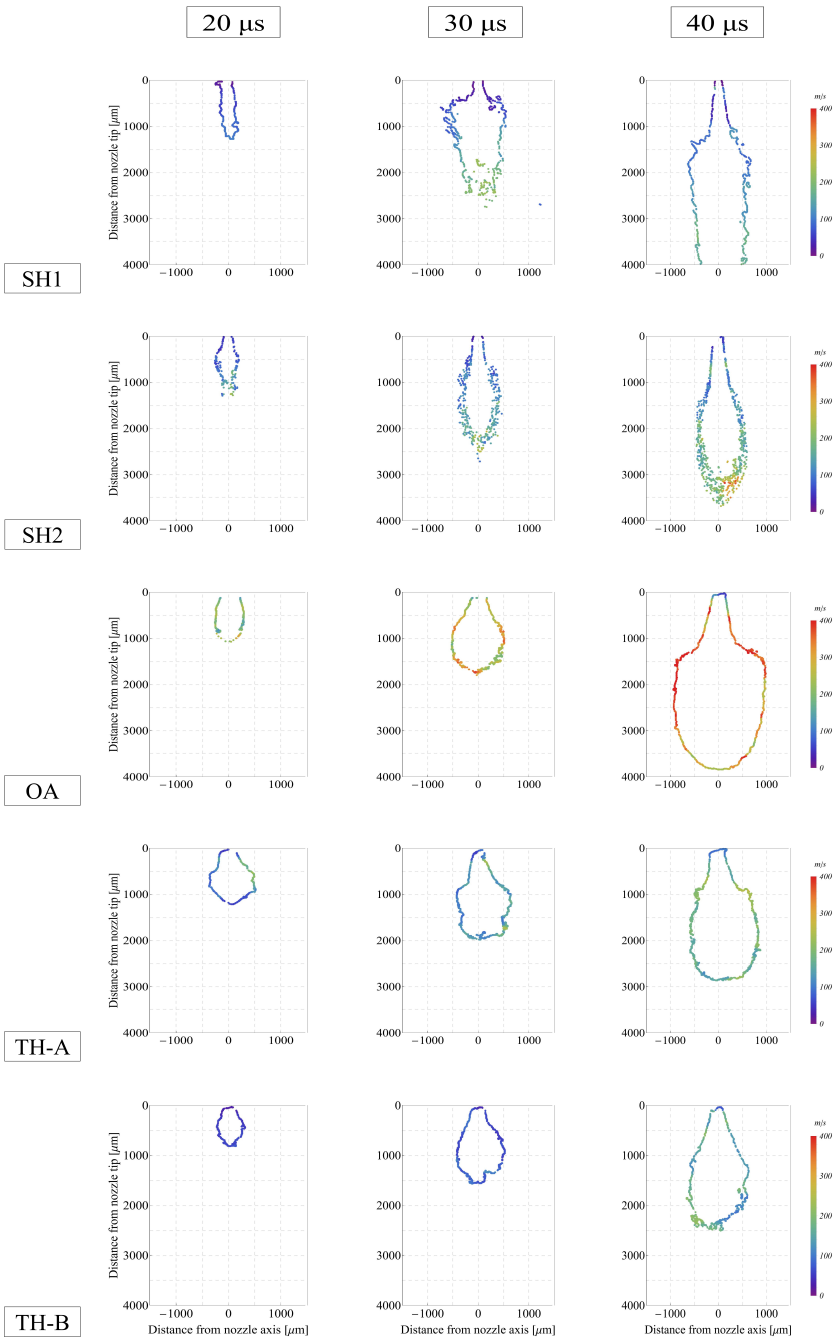

Figure 4.1: *Mean velocity magnitude for near-field sprays generated by five different orifices at 800 bar*

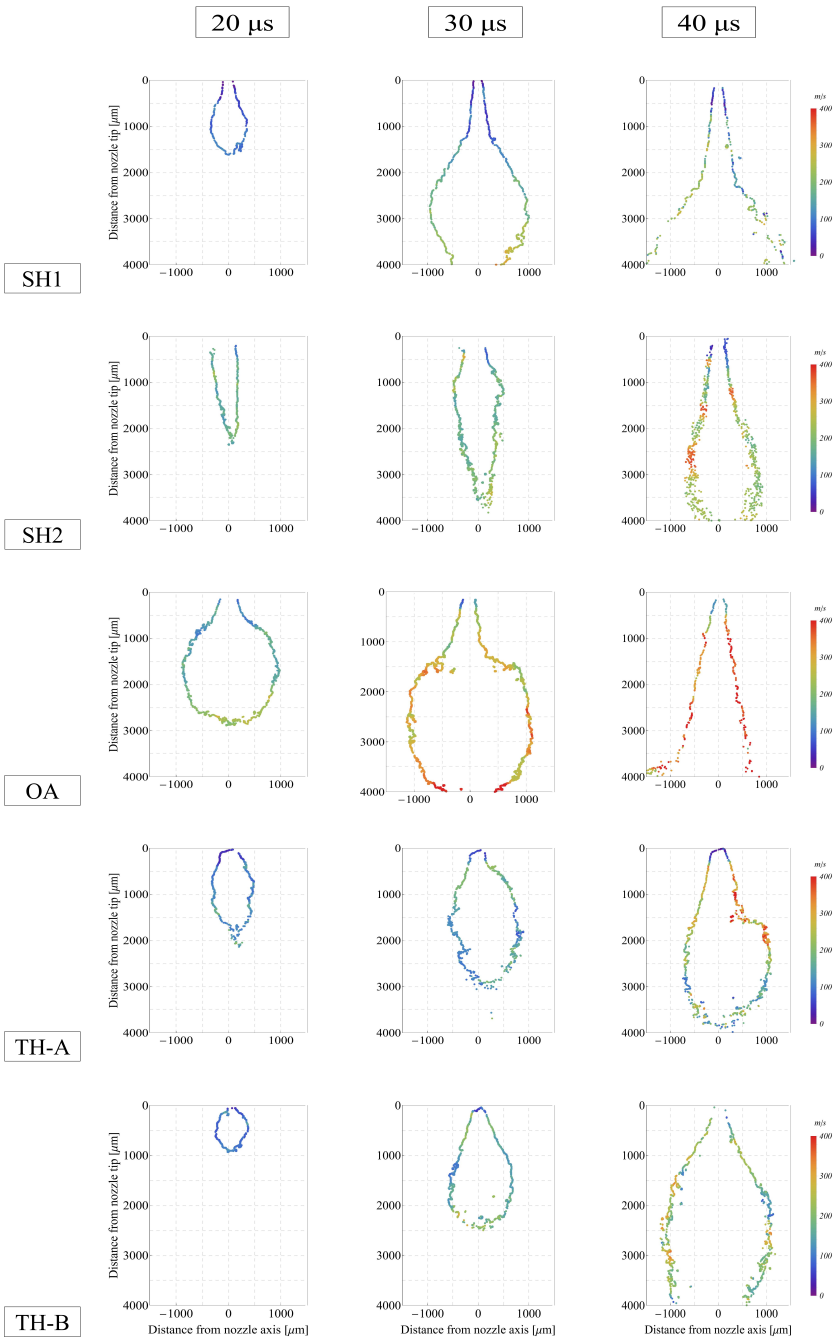

Figure 4.2: *Mean velocity magnitude for near-field sprays generated by five different orifices at 1600 bar*

two-hole nozzles become smaller, and Figure 4.3 confirms this view. This phenomenon is also evident when comparing the nozzles SH1 and SH2; this may contribute to higher spray penetration of the nozzle with a smaller orifice at corresponding time steps.

4.3 Effect of injection pressure

Figures 4.1 and 4.2 show velocity profiles at 800 bar and 1600 bar respectively. According to these figures, injection pressure mainly influences the velocity and acceleration of the spray but it has a negligible effect on the overall spray profile, especially at steady-state. Nevertheless, increasing injection pressure beyond a critical value can also affect the prevailing spray profile in nozzle geometries that are more prone to cavitation. As discussed earlier, increasing the injection pressure boosts the spray deflection in asymmetric orifices. In addition, raising injection pressure impacts the near-field spray profile for the cylindrical nozzle and makes it slightly wider. Therefore, the effect of pressure on the spray profile can be considered as a secondary effect. Furthermore, one can predict that the higher velocity provoked by raised injection pressure enhances the break-up process, resulting in a significant effect on spray characteristics in the far-field, including the maximum liquid penetration length and Sauter-mean diameter.

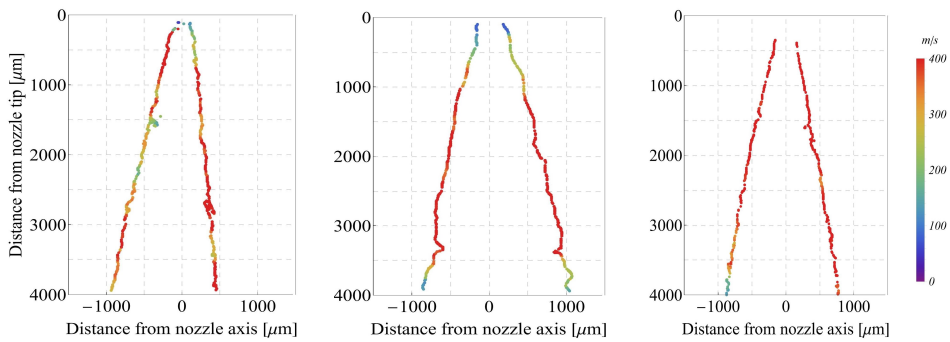

(a) OA (b) TH-A (c) TH-B

Figure 4.3: *mean velocity magnitudes for near-field sprays at 800 μs after start of injection under 1600 bar of injection pressure.*

Comparing nozzle SH1 with other nozzles indicates that convergent orifices (larger k-factor) generate narrow sprays, while the flow tends to expand more in the radial direction in a cylindrical orifice. According to the results, it is clear that increasing the injection pressure intensifies the spray expansion in nozzle SH1, which is likely due to an increased cavitation level. This matches the trends discussed in Chapter 2, where higher pressure drop and low k-factor are shown to increase the probability of cavitation and its intensity.

The spray profile at a quasi-steady state for the off-axis nozzle (Figure 4.3(a)) reveals that the spray deviates towards the left side (the side with a sharper inlet edge). This trend is also visible for the second orifice of the TH nozzle (TH-B) but is more gentle. In addition, the overall velocity magnitude on the left side appears to be lower than on the other side. The presence of the sharp edge at the left side probably causes this. As mentioned in Chapter 2, cavitation starts with the flow separation from the orifice wall; if an asymmetrical boundary layer forms inside the orifice, a so-called "hydraulic flip" can arise and cause deflection in the spray profile [42]. Therefore, it is likely that a more significant asymmetry at the orifice leads to a more extensive deflection in the spray profile. Moreover, that could be the reason for the lower deviation in spray direction in TH orifices than the OA nozzle (Figures 4.3(b) and 4.3(c)).

4.4 Statistical analysis

As stated in Chapter 3, we measure the spray kinematics based on 150 to 200 statistical samples. Figure 4.4 shows the superimposition of all extracted velocity magnitudes for spray at 800 μs ASOI and 1600 bar pressure for the OA nozzle. This image is an example to show the non-uniform velocity distribution even in a close neighborhood of any coordinate. Perhaps shot-to-shot variations in spray profiles and initial conditions, including pressure fluctuations and the amount of trapped fuel in the sac, could be the source of variations in velocity magnitudes. In addition, correlation mismatches might also exist because the correlation coefficient, which describes the similarity between the two samples, is never set to 100%. However, the probability of a correlation mismatch is relatively low. As mentioned earlier, the velocity magnitude of each point on the spray periphery consists of the mean value of all extracted velocity magnitudes in the neighborhood of that point. Therefore, we should analyze the statistical data to estimate the reliability of the results.

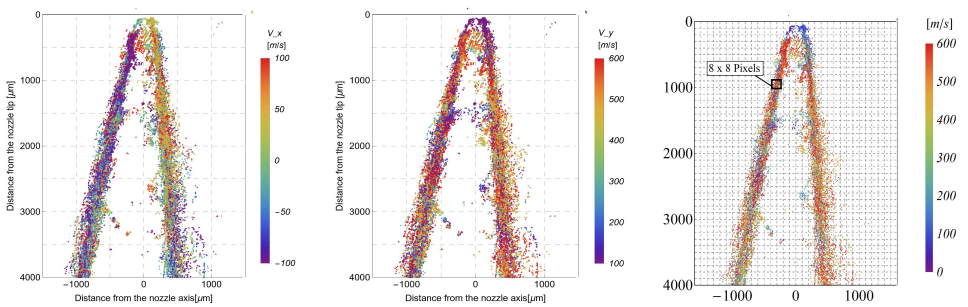

Figure 4.4: *All extracted velocity data for the OA nozzle at 800 μs after start of injection. a) radial velocity components, b) axial velocity components, and c) velocity magnitudes.*

In order to analyze the results, we present them in the form of histograms. As an example, Figure 4.5(a) displays the population distribution of all velocities within an 8×8 pixels distance from a random coordinate (x=43, y=321 pixel) at a particular case (800 μs, 1600 bar). At the first glance, we notice there is a relatively large range of velocity values and a large variance. However, the most population exists between 450 to 600 m/s. In order to automatically detect the range with the highest population, we examined the effect of data filtration. Figure 4.5(b) and 4.5(c) depict the histogram of velocity data after mean and median filtering, respectively. Table 4.1 also provides the primary statistical information for each filtering method. These results show that applying median filtering emphasizes the range with the most population, and the calculated average of those data will be closer to the highest population range. In addition, if we eliminate the outliers from the averaging process, the calculated mean (Trimmed mean) will be even placed in the middle of that range. Therefore, we can enhance the obtained results for model validation by applying the median filter and eliminating the outliers for averaging.

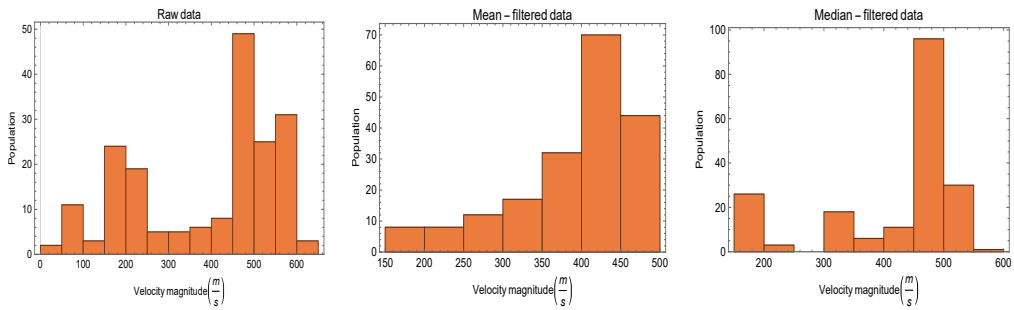

(a) (b) (c)

Figure 4.5: *Histograms of extracted velocity populations for OA nozzle at the coordinate of [43, 321] pixel , 800 μs after start of injection and 1600 bar. a) raw data, b) mean-filtered data, c) median-filterd data.*

Table 4.1: statistical evaluation of filtering velocity data

Data type	**Mean value**	**Median value**	**Trimmed mean**	**Largest population**
Raw	390	445	396	450-500
Mean-filtered	391	419	396	450-500
Median-filtered	416	468	422	450-500

5 Future work

The obtained velocity data will be used to compare and validate simulation models. After validating the model, there will be a possibility of establishing a correlation between the simulated in-nozzle flow and the near-field flow characteristics within the two-hole and off-axis nozzles to understand the effect of particular nozzle geometries on the internal flow.

The results of this study can be further improved by increasing the number of statistical samples. In addition, it is worth studying other parameters that affect spray dynamics, such as ambient pressure and fuel properties. For this purpose, a new experimental campaign will be performed in a high-pressure chamber to study the back-pressure effect. A new injector holder must be designed and fabricated to mount the injector on the high-pressure chamber. This new injector holder should make it possible to mount the injector with different orientations. Therefore, it enables to capture of spray images on different spatial planes around the orifice axis. By measuring and interpolating the spray velocity profiles on several intersecting normal planes, a 360° velocity profile for the spray can be constructed.

Finally, the non-reactive spray behavior in the far-field and even the mixing and combustion phase of the spray within the prototype nozzles can be evaluated with the aid of other common methods in spray research, including PIV and PLIF.

Bibliography

[1] Joanna Nowakowska-Grunt and Monika Strzelczyk. “The current situation and the directions of changes in road freight transport in the European Union”. In: *Transportation Research Procedia*. 3rd International Conference "Green Cities – Green Logistics for Greener Cities", Szczecin, 13-14 September 2018 39 (2019).

[2] Ana Carolina Rodrigues Teixeira et al. “Alternative fuel technologies emissions for road heavy-duty trucks: a review”. In: *Environmental Science and Pollution Research* 28.17 (2021).

[3] Arun S. K. Raju, Barry R. Wallerstein, and Kent C. Johnson. “Achieving NOx and Greenhouse gas emissions goals in California’s Heavy-Duty transportation sector”. In: *Transportation Research Part D: Transport and Environment* 97 (2021).

[4] Christopher J. Polonowski et al. “An Experimental Investigation of Low-Soot and Soot-Free Combustion Strategies in a Heavy-Duty, Single-Cylinder, Direct-Injection, Optical Diesel Engine”. In: *SAE International Journal of Fuels and Lubricants* 5.1 (2011).

[5] Gang Li, Chunhua Zhang, and Yangyang Li. “Effects of diesel injection parameters on the rapid combustion and emissions of an HD common-rail diesel engine fueled with diesel-methanol dual-fuel”. In: *Applied Thermal Engineering* 108 (2016).

[6] Wei Chen et al. “Effect of injection strategy on fuel-air mixing and combustion process in a direct injection diesel rotary engine (DI-DRE)”. In: *Energy Conversion and Management* 154 (2017).

[7] Sibendu Som et al. “Effect of nozzle orifice geometry on spray, combustion, and emission characteristics under diesel engine conditions”. In: *Fuel* 90.3 (2011).

[8] Safiullah, Keiya Nishida, and Youichi Ogata. “Evaporation and mixture formation characteristics of diesel spray under various nozzle hole size and injection pressure condition employing similar injection rate profile”. In: *International Communications in Heat and Mass Transfer* 123 (2021).

[9] Chengjun Du, Mats Andersson, and Sven Andersson. “Effects of Nozzle Geometry on the Characteristics of an Evaporating Diesel Spray”. In: *SAE International Journal of Fuels and Lubricants* 9.3 (2016).

[10] John E. Dec. *A Conceptual Model of DI Diesel Combustion Based on Laser-Sheet Imaging**. SAE Technical Paper 970873. ISSN: 0148-7191, 2688-3627. Warrendale, PA: SAE International, 1997.

[11] Thomas Wintrich and Meike Keller. “Basic principles of diesel fuel injection”. In: *Diesel Engine Management: Systems and Components*. Ed. by Konrad Reif. Wiesbaden: Springer Fachmedien, 2014. ISBN: 978-3-658-03981-3.

[12] ROLF DENEYS REITZ. “Atomization and Other Breakup Regimes of a Liquid Jet.” ISBN: 9798661024862. PhD thesis. United States – New Jersey: Princeton University. 336 pp.

[13] Gunnar Stiesch. *Modeling engine spray and combustion processes*. Heat and mass transfer. Springer, 2003. ISBN: 978-3-540-00682-4.

[14] Kuppuraj Rajamanickam, Achintya Mukhopadhyay, and Saptarshi Basu. “On Primary Atomization in Propulsive Device Fuel Injectors—A Short Review”. In:

Droplets and Sprays : Applications for Combustion and Propulsion. Ed. by Saptarshi Basu et al. Energy, Environment, and Sustainability. Singapore: Springer, 2018. ISBN: 978-981-10-7449-3.

[15] Arthur H. Lefebvre and Vincent G. McDonell. "Basic Processes in Atomization". In: *Atomization and Sprays*. 2nd ed. Num Pages: 38. CRC Press, 2017. ISBN: 978-1-315-12091-1.

[16] P. H. Schweitzer. "Mechanism of Disintegration of Liquid Jets". In: *Journal of Applied Physics* 8.8 (1937).

[17] M. J. McCarthy and N. A. Molloy. "Review of stability of liquid jets and the influence of nozzle design". In: *The Chemical Engineering Journal*. An International Journal of Research and Development 7.1 (1974).

[18] Luka Lešnik et al. "The influence of in-nozzle cavitation on flow characteristics and spray break-up". In: *Fuel* 222 (2018).

[19] F. Payri et al. "A contribution to the understanding of cavitation effects in Diesel injector nozzles through a combined experimental and computational investigation". In: *Computers & Fluids* 58 (2012).

[20] J. Javier López et al. "A comprehensive study on the effect of cavitation on injection velocity in diesel nozzles". In: *Energy Conversion and Management*. IREC 2011, The International Renewable Energy Congress 64 (2012).

[21] Zuo-Yu Sun et al. "Numerical investigation on effects of nozzle's geometric parameters on the flow and the cavitation characteristics within injector's nozzle for a high-pressure common-rail DI diesel engine". In: *Energy Conversion and Management* 89 (2015).

[22] Felix Landhäußer et al. "Overview of common-rail systems". In: *Diesel Engine Management: Systems and Components*. Ed. by Konrad Reif. Wiesbaden: Springer Fachmedien, 2014. ISBN: 978-3-658-03981-3.

[23] Sandro Soccol and Werner Brühmann. "High-pressure components of common-rail system". In: *Diesel Engine Management: Systems and Components*. Ed. by Konrad Reif. Wiesbaden: Springer Fachmedien, 2014. ISBN: 978-3-658-03981-3.

[24] F. J. Salvador et al. "Analysis of the combined effect of hydrogrinding process and inclination angle on hydraulic performance of diesel injection nozzles". In: *Energy Conversion and Management* 105 (2015).

[25] Yu Jin et al. "Comparison of diesel spray with small injection amount between single-hole and multi-hole injectors: Results under same rail pressure and similar injection rate". In: *International Communications in Heat and Mass Transfer* 118 (2020).

[26] Weidi Huang et al. "Eccentric needle motion effect on near-nozzle dynamics of diesel spray". In: *Fuel* 206 (2017).

[27] Yijie Wei et al. "Time-resolved measurement of the near-nozzle air entrainment of high-pressure diesel spray by high-speed micro-PTV technique". In: *Fuel* 268 (2020).

[28] Raul Payri et al. "The effect of nozzle geometry over internal flow and spray formation for three different fuels". In: *Fuel* 183 (2016).

[29] Meshack Hawi et al. "Effect of injection pressure and ambient density on spray characteristics of diesel and biodiesel surrogate fuels". In: *Fuel* 254 (2019).

[30] Balaji Mohan et al. “Macroscopic spray characterization under high ambient density conditions”. In: *Experimental Thermal and Fluid Science* 59 (2014).
[31] F. J. Salvador et al. “Experimental analysis of the injection pressure effect on the near-field structure of liquid fuel sprays”. In: *Fuel* 292 (2021).
[32] Chenglong Tang et al. “Experimental study on the effect of injector nozzle K factor on the spray characteristics in a constant volume chamber: Near nozzle spray initiation, the macroscopic and the droplet statistics”. In: *Fuel* 202 (2017).
[33] Ming-Chia D Lai Philip J Dingle. *Diesel Common Rail and Advanced Fuel Injection Systems*. SAE International, 2005. ISBN: 978-0-7680-2200-1.
[34] Raditya Hendra Pratama, Weidi Huang, and Seoksu Moon. “Unveiling needle lift dependence on near-nozzle spray dynamics of diesel injector”. In: *Fuel* 285 (2021).
[35] David Sedarsky et al. “Fast-framing ballistic imaging of velocity in an aerated spray”. In: *Optics Letters* 34.18 (2009).
[36] David Sedarsky et al. “Velocity measurements in the near field of a diesel fuel injector by ultrafast imagery”. In: *Experiments in Fluids* 54.2 (2013). arXiv: 1301.6593.
[37] Mark A. Linne et al. “Ballistic imaging of liquid breakup processes in dense sprays”. In: *Proceedings of the Combustion Institute* 32.2 (2009).
[38] Lyle M. Pickett et al. “Comparison of Near-Field Structure and Growth of a Diesel Spray Using Light-Based Optical Microscopy and X-Ray Radiography”. In: *SAE International Journal of Engines* 7.2 (2014).
[39] Zachary Falgout et al. “Gas/fuel jet interfaces under high pressures and temperatures”. In: *Fuel* 168 (2016).
[40] Harsh Purwar et al. “Collinear, two-color optical Kerr effect shutter for ultrafast time-resolved imaging”. In: *Optics Express* 22.13 (2014). arXiv: 1502.03350.
[41] David Sedarsky et al. “Planar velocity analysis of diesel spray shadow images”. In: *arXiv:1203.5347 [physics]* (2012). arXiv: 1203.5347.
[42] Celia Soteriou, Richard Andrews, and Mark Smith. “Direct Injection Diesel Sprays and the Effect of Cavitation and Hydraulic Flip on Atomization”. In: International Congress & Exposition. 1995.

Abbreviations

$ASOI$	After the Start Of Injection
BI	Ballistic Imaging
CFD	Computational Fluid Dynamics
CI	Compression Ignition
CO	Carbon monoxide
$CO2$	Carbon dioxide
D	Orifice Diameter
HC	Hydrocarbon
HPC	High Pressure Connector
$HSOI$	Hydraulic Start Of Injection
$ICCD$	Intensified Charge-Coupled Device
L	Orifice Length
NOx	Nitrogen Oxides
OA	Off-Axis nozzle
Oh	Ohnesorge Number
OKE	Optical Kerr Effect
PIV	Particle Image Velocimetry
$PLIF$	Planar Laser Induced Fluorescence
Re	Reynolds Number
$SH1$	Single-Hole nozzle 1
$SH2$	Single-Hole nozzle 2
SI	Spark Ignition
SMD	Sauter Mean Diameter
SOI	Start of Injection
$TH-A$	Two-Hole nozzle- orifice A
$TH-B$	Two-Hole nozzle- orifice B
TH	Two-Hole nozzle
We	Weber Number
XPI	eXtra high Pressure Injection

Publication A

Near-field spray velocity and development in single-hole diesel injector

ILASS-Americas 31st Annual Conference on Liquid Atomization and Spray Systems, Madison, WI, May 2021

Near-field spray velocity and development in single-hole diesel injector

M. Nikouei[1,2*] and D. Sedarsky[1]
[1]Division of Combustion and Propulsion Systems
Chalmers University of Technology
Gothenburg, Sweden
[2]Scania AB
Södertälje, Sweden

Abstract

High-pressure atomizing sprays are essential for fuel/air mixing in diesel combustion applications and variability in the spray formation process can significantly affect engine efficiency and emissions. In this work we apply two-pulse collinear ballistic imaging to a high-pressure Diesel spray generated by single-orifice nozzles with different inlet geometries and outlet diameters. We image the near-field and track spatially resolved droplets and liquid interface structure to map velocity trends from start-of-injection to fully developed spray in a range of injection pressures. A number of studies have examined the effect of fuel injection conditions on combustion quality and mixing and consistent far-field trends in spray morphology. Although a number of approaches are available to measure droplet velocities in the developed spray, optical measurements applied in the near-field remain challenging due to the scattering interference from small fuel droplets. In this work, we apply a time-gated ballistic imaging to suppress multiply-scattered light and obtain spatially resolved image data which can be analyzed to track fluid motion in the developing spray. The results show that higher injection pressure increases turbulence level, instabilities and varieties in near-field velocity profiles and spray width. In addition, increasing injection pressure, reduces time for nozzle opening delay and spray development. We have also found that overall velocity is higher for the nozzle with smaller hole diameter and nozzle geometry is the more dominant factor than injection pressure for radial spray expansion.

*Corresponding Author: mohnik@chalmers.se

Introduction

Increasing demand for transportation has led to an increase in pollutants and greenhouse gases and one way to deal with this problem is to improve the efficiency of combustion engines and control the combustion products. In internal combustion engines, various processes are involved in the conversion of chemical energy into mechanical energy, among which fuel injection is a great of importance because it has a commanding influence on the mixing and combustion quality.

In general, spray characteristics are defined by penetration length, cone angle, break-up length and Sauter mean diameter, which affecting mixing and combustion characteristics [1]. Various research have been conducted to study the effects of internal and external conditions on spray characteristics. Gopinath et al. [1] made a review about the effects of ambient conditions on spray characteristics. In addition, several studies have focused on the effects of fuel properties [2, 3], nozzle geometry [3, 4, 5] and injection pressure [6, 7]. Any variations in spray characteristics might have an influence on the mixing and the combustion quality; for instance, larger spray con angle enhances air entrainment and mixing [8].

In addition to macroscopic spray properties, the velocity of the injected fuel and droplets is another important criterion that enhances our knowledge about spray and fuel-air mixing control. In addition, the velocity field can provide a more clear explanation about the physical properties of the spray. On the other hand, the aerodynamics force exerted on the fuel droplets, which is one of the most important mechanisms of the secondary break-up, is exponentially proportional to the velocity of the droplets [9], and as a result, the fuel jet velocity field can provide a better estimation of the secondary break-up characteristics and it can also be used as a reference for evaluating and validating simulation models.

According to a recent study [10], there are several stages between the start of injection and combustion. The first phase, which is called non-reactive phase, is of great importance because the mixing process takes place at this phase and affects the next stages. Another classification [11] states that non-reactive spray can be divided into four regions:

- internal nozzle flow
- the near-field region, where primary break-up is observed.
- the far-field region, where secondary break-up occurs
- spray-wall interaction region.

It is more challenging to study the near-field spray due to its high fuel flow density and too small field of view. Most of relevant research works, have studied the far-field while according to the author's knowledge, investigations about the near-field are still limited. There are common methods to measure velocity field in flows such as Particle Image Velocimetry (PIV) [12] or Particle Tracking Velocimetry (PTV) [8]. These measurements were mostly performed by using seeding particles. Nevertheless, Payri et al. [13] have implemented PIV without seeding particles but only in the far-field. Another study group [14], have used another method called Particle/Droplet Image Analysis (PDIA) to evaluate particle's velocity and size; however, their study is also limited to the far-field. Therefore, as [15] states, it seems quite challenging to measure velocity at near-field without seeding particles; because either no droplet is formed or they are too small to be detected. Nevertheless, they successfully measured near-field velocity by implementing Doppler Global Velocimetry (DGV). These methods are mostly based on high-speed photography with different techniques and optical setup. some of the common methods are reviewed by M.Linne [16]. Among those imaging methods ballistic imaging is our method of interest because the ultra-fast optical shutter with the time scale of picoseconds is able to reduce the motion blur effect and provides sharper images with higher spatial resolution [17].

In this work we aim to perform statistical velocity measurements on the near-field spray for two different single hole nozzles over a range of injection pressures by using co-linear ballistic imaging [18] as the imaging tool.

Experimental Setup

The method of study is based on statistical analysis of spray kinematics in the near-field region by using a dense-media imaging approach, known as ballistic imaging to visualize the liquid structures buried in the dense cloud of droplets surrounding a diesel spray. Image acquisition method is based on collinear ballistic imaging [18]. It is expected to achieve high resolution images using this method so that the arrangement of fuel ligaments in the spray periphery appear sharp enough to find spray features and track them accurately in each image pair. Fig. 1 displays a schematic of the optical setup and its main elements. In this setup, there are two cross polarizers and a cell (with the thickness of 5 mm) filled by carbon disolfide (CS_2). This combination provides

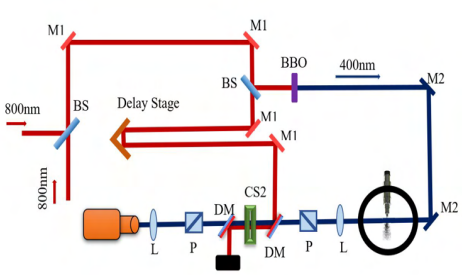

Figure 1. A schematic view of image acquisition system configuration. M1: 800 nm mirror, M2: 400 nm mirror, BS: Beam Splitter, P: Polarizer, L: Lens, DM: Dichroich Mirror.

an ultra-fast shutter to reduce motion blur effect. In this setup, light can be transmitted through the second polarizer only if CS_2 operates as a birefringence material and changes the light polarization by 90°. When a laser pulse energizes CS_2, it activates the birefringence feature for a time period of 2 ps. For this purpose, the laser beam is divided in two parts using a beam splitter. The portion with lower energy is used as the imaging beam while the other one plays the switching role to activate CS_2 birefringence. In order to minimize the interaction between the two beams, the imaging beam frequency is doubled by transmitting through a Barium Borate Oxide (BBO) crystal.

The light source is supplied by two regenerative amplifiers that are seeded by a common Ti-Sapphire oscillator and the resulting beam is a pair of femtosecond pulses that are generated every 1 ms with the wavelength of 800 nm. The experiments have been done with a double laser pulses with dwell time of 560 ns. This provides the opportunity to study spray kinematics, given that sufficient number of samples collected for statistical velocimetry. The injector is mounted on a constant-volume chamber, which can be pressurized up to 30 bar, however, experiments have been done in atmospheric conditions. A fuel pipe connects the injector fuel line to a common-rail system. The rail is pressurized by a fuel pump with the maximum capacity of 3000 bar. For each injection event, an injector driver excites the injector solenoid for a certain time period up to 6 ms and it is controlled by a signal/delay generator.

Table 1. Experimental conditions

Parameter	Value	Unit
Rail pressure	800, 1200, 1600	bar
Back pressure	atm	-
Ambient temperature	294	K
Injection duration	2	ms

Table 2. Nozzles specifications

Nozzle	N_1	N_2
Outlet diameter [μm]	180	140
Orifice Length [mm]	1	1
k-factor	2	0
Hydro-grinding level [%]	30	30

The image acquisition device that is used for experiments is an ICCD PI-Max 4 featuring double frame function and resolution of 1024×1024 pixels. Each frame is synchronized with the corresponding laser pulse using the delay generator device. This optical setup provides spacial resolution of 8.33 μm per pixel.

As Table 1 indicates experimental plan and conditions, three injection pressures were used for two different single-hole nozzles. These nozzles have been selected to evaluate and compare the effect of outlet diameter and k-factor on the spray near-field. Table 2 presents nozzles specifications. Both nozzles have only one orifice, located parallel to the injector axis with 30 % of hydro-grinding.

Spray images are taken at two stages. First, it is necessary to find the time instant, when the liquid fuel is about to exit the nozzle. This time instance is called Hydraulic Start Of Injection (HSOI). For this purpose, 20 images are taken with a temporal resolution of 1 μs before and after the estimated nozzle opening delay. Second, it is interesting to observe spray behaviour over the transient phase from the emergence of liquid fuel until it exceeds the field of view. Therefore, we took image sets from 20 to 50 μs after HSOI with resolution of 5 μs. Since there is relatively high instabilities in the transient phase, in order to be able to perform accurate analysis, we have to increase the number of statistical samples as much as possible. In this experiments, we took over 200 image pairs per each time instant.

Data processing and analysis

Once all the images collected, it is first necessary to prepare images for measuring spray kinematics. In order to remove noise from the images, we subtract an averaged background from the images. Then, we apply a fast normalized cross-correlation

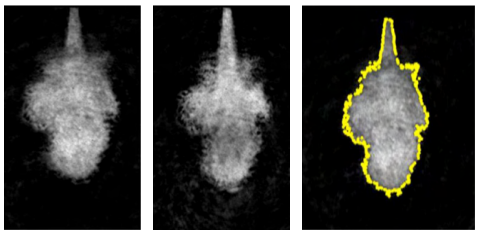

(a) $t = t_1$ (b) $t = t_1 + 560ns$ (c) Target points

Figure 2. Example of one image pair taken with a time difference of 560 ns and distribution of target points

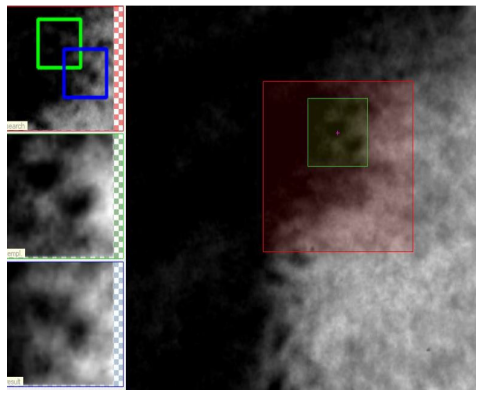

Figure 3. An example of spray tracking. On the left side, green square shows the position of the template in the first image and the blue square is the matched template from the second image. The red box indicates the search field.

to match and track liquid structures using OpenCV library. This method has been proved earlier with a slightly different imaging method [19]. In this method, first, several target points are introduced as the origin of matching templates. These points are distributed randomly across the spray periphery (Fig. 2(c)). The number of these points are chosen proportional to the average penetration length of the spray at the respective time instant. The template window, contains information of the pixels intensities and their texture in vicinity of each target point. In the next step, it is required to find the most similar pattern to match with this information through a specific domain in the second image (taken at $t_2 = t_1 + dt$). That domain is called search field and is a sub-grid region around the template with the area of 2 to 3 times greater than the template window. The distance between the initial target point and the origin of the matched template is equivalent to the displacement vector and represents the fluid motion around the target point. Fig. 3 shows an example of matched templates for a random target point.

Displacement of liquid structures over a very short dwell time (560 ns) between the images, presents an estimation of the instantaneous velocity in vertical and horizontal directions at specific time instants. It should be noted that in order to calculate the overall velocity magnitude, we have considered the velocity in the third direction (normal to the plane) equal to the lateral velocity component. Since spray images are not identical and have a great variety of shapes, we build an averaged image as the overall shape of the spray. As in the previous steps, we consider target points on the averaged spray periphery. Then, we calculate the mean velocity for each point using all available velocity data (calculated for all image pairs at corresponding time instant) as the statistical population. For this purpose, the mean velocity at each target point will be equal to the average of all velocity vectors that are available within a certain distance (8 pixels) from that point; given that the number of data for averaging must be higher than 50. This eliminates the points, where either the probability of observing spray is low or there is high uncertainty in velocity calculation.

Results and discussion

The results of these experiments are illustrated in the form of 2D velocity maps in Figs. 4 to 7. In each plot, the origin represents the position of the injector tip, vertical axis indicates the distance from the nozzle tip and horizontal axis shows the radial distance from the nozzle axis. The points on each plot form the average shape of spray at corresponding time instances and their colours indicate overall velocity magnitude. We analyse the results from two perspectives: the effects of injection pressure and the effect of nozzle geometry. In addition to the velocity profile, we qualitatively compare and discuss the penetration rate, overall shape of the spray and development patterns at near-field.

Figs. 4 and 6 illustrate the spray velocity profile for nozzle N1 under different injection pressures within 20 to 45 μs after HSOI. The first thing that we should note is the difference between the appearance of spray in those plots.

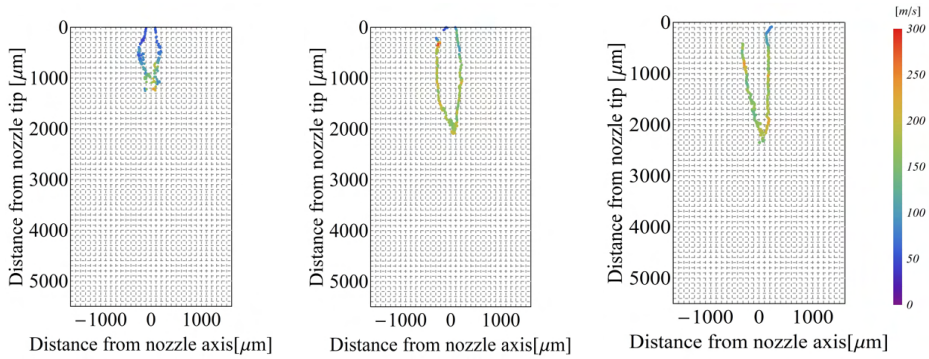

(a) $P = 800\ bar,\ t = 20\mu s$ (b) $P = 1200\ bar,\ t = 20\mu s$ (c) $P = 1600\ bar,\ t = 20\mu s$

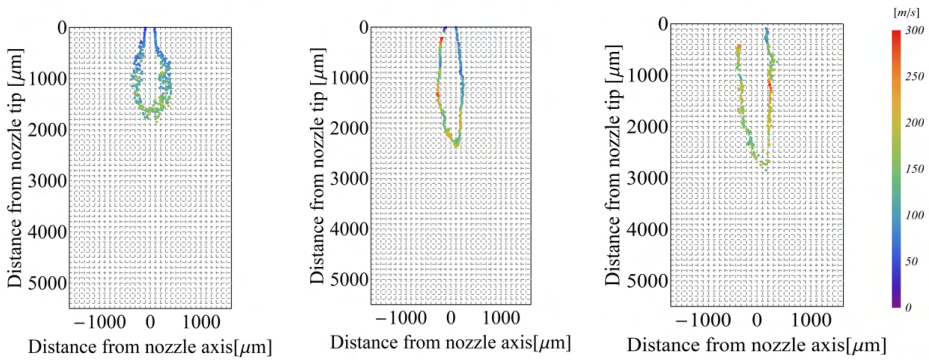

(d) $P = 800\ bar,\ t = 25\mu s$ (e) $P = 1200\ bar,\ t = 25\mu s$ (f) $P = 1600\ bar,\ t = 25\mu s$

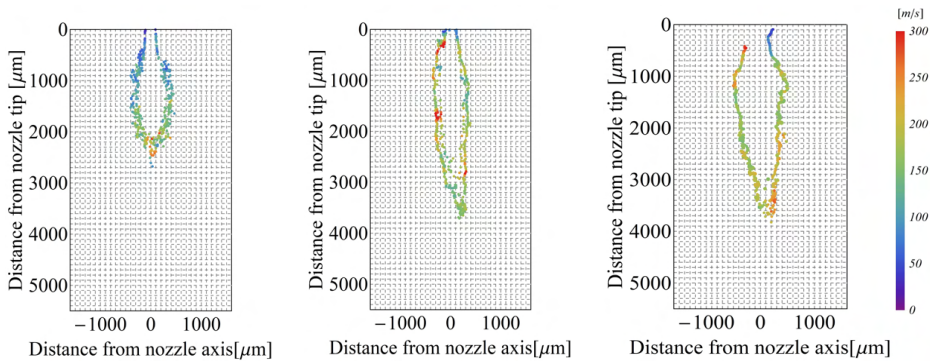

(g) $P = 800\ bar,\ t = 30\mu s$ (h) $P = 1200\ bar,\ t = 30\mu s$ (i) $P = 1600\ bar,\ t = 30\mu s$

Figure 4. Near-field Velocity profiles of sprays generated by nozzle N1 at 3 different injection pressures from 20 to 30 μs after HSOI

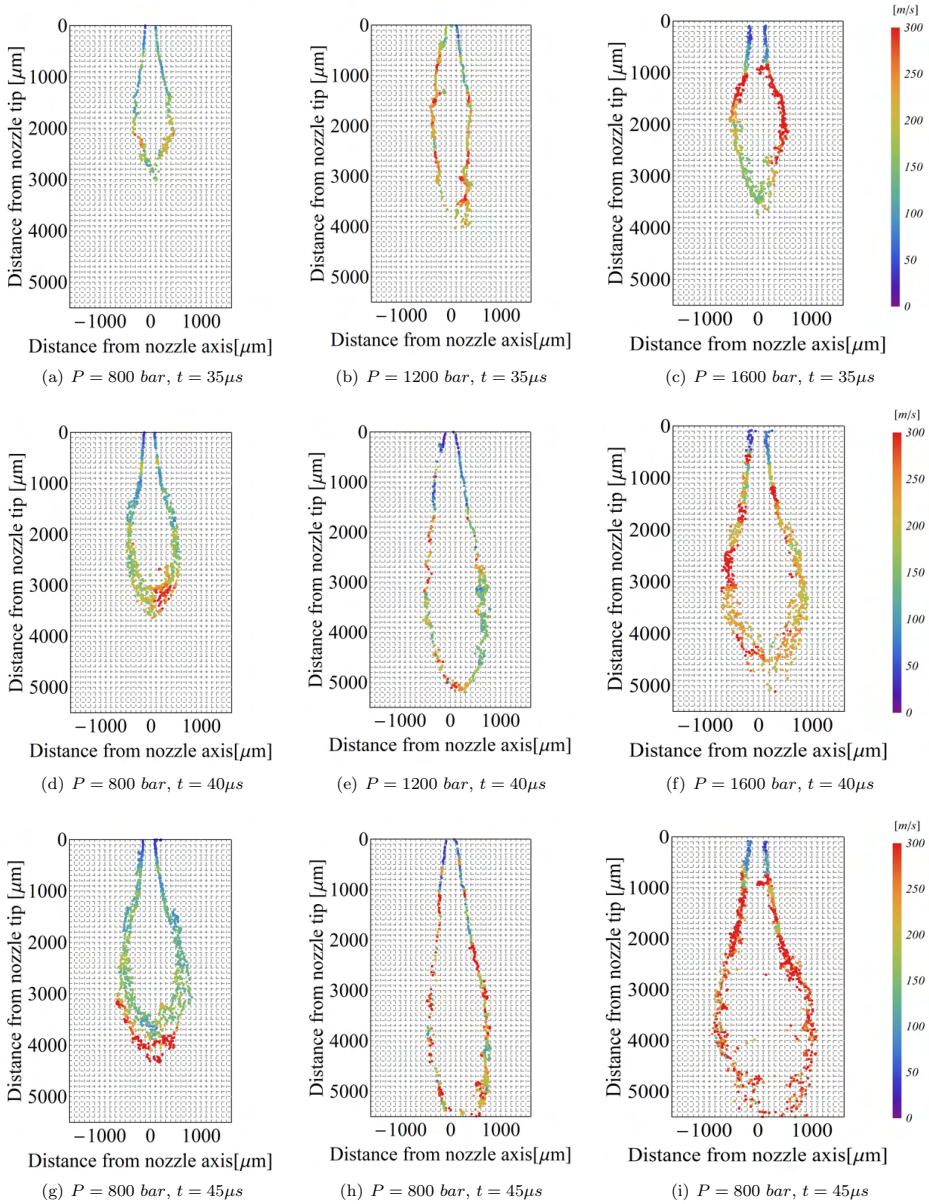

(a) $P = 800\ bar$, $t = 35\mu s$ (b) $P = 1200\ bar$, $t = 35\mu s$ (c) $P = 1600\ bar$, $t = 35\mu s$

(d) $P = 800\ bar$, $t = 40\mu s$ (e) $P = 1200\ bar$, $t = 40\mu s$ (f) $P = 1600\ bar$, $t = 40\mu s$

(g) $P = 800\ bar$, $t = 45\mu s$ (h) $P = 800\ bar$, $t = 45\mu s$ (i) $P = 800\ bar$, $t = 45\mu s$

Figure 5. Near-field velocity profiles of sprays generated by nozzle N1 at 3 different injection pressures from 35 to 45 μs after HSOI

At 800 and 1600 bar, the spray looks slightly wider than at 1200 bar and resembling a mushroom shape. It is noteworthy that the spray penetration at 1200 bar is very close to 1600 bar condition and even slightly higher at some of the time instants. This becomes more interesting when we realize that generally, the velocities at 1600 bar is higher than the corresponding points at 1200 bar. Therefore, we may infer that at 1600 bar pressure, the radial velocity component increases more than the axial component and as a result, the spray becomes slightly wider while penetrations is not affected.

Upon closer look, one can see that the spray leading edge tends to deviate towards the positive direction of the horizontal axis. In addition, increasing injection pressure amplifies this deviation. According to Figs 4 and 5, at 800 bar, velocity magnitudes on both sides of the nozzle axis are approximately equal, at least during the initial time instants. Therefore, velocity balance at spray margins prevents large spray deviation. On the other hand, at higher injection pressures, we can observe that the velocity profiles on both sides of the nozzle axis are not symmetrical and there are fluctuations in velocity magnitude on each side. It has been known that higher pressure intensifies cavitation and pressure fluctuations [20] and this, could be an explanation for velocity fluctuations across the spray periphery. In addition, Salvador et al.[21] confirmed that higher pressure increases turbulence intensity and consequently, the variety of spray shapes becomes greater. Diversity in spray shapes is in fact due to the instabilities and variations in velocity profiles.

In the region very close to the nozzle tip (0 to 0.5 mm), velocity magnitude is significantly lower than other spray regions and this, is evident in all plots. Since the region close to the orifice features a liquid column with a very sharp interface between liquid and gas, only very small amounts of liquid are found outside the column. These small amounts are mostly slow moving remnants from start of injection. The column itself moves fast, but its structures is optically dense and it is challenging to capture central structures. As the result, the velocities extracted at the periphery close to the orifice are small in magnitude.

Another effect of injection pressure is changing the Nozzle Opening Delay (NOD). The higher the pressure, the less the NOD is. It also seems that the transient phase in spray development becomes shorter in time. By comparing Figs. 5(g), 5(h), 5(i), we observe that velocities at different positions increase and get closer to each other at 45 μs, specially with injection pressure of 1600 bar. When the injector needle is fully open, the overall spray velocity is expected to reach the maximum.

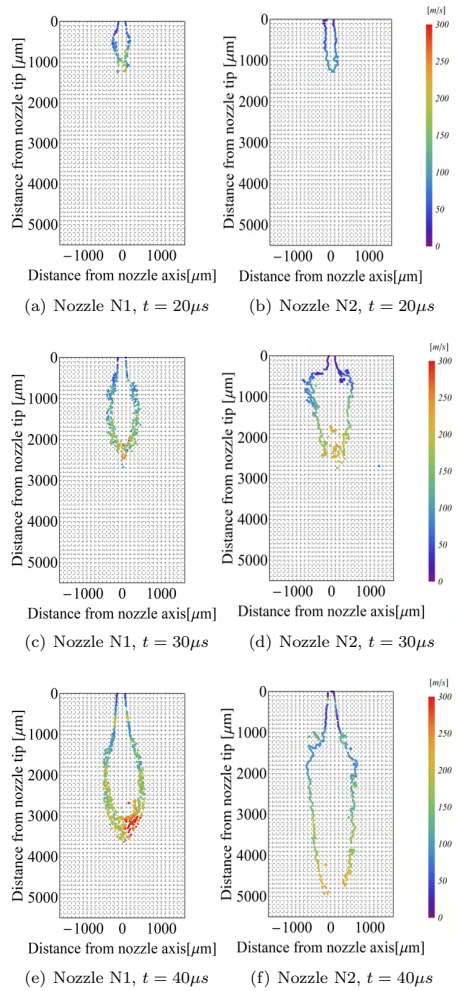

(a) Nozzle N1, $t = 20\mu s$ (b) Nozzle N2, $t = 20\mu s$

(c) Nozzle N1, $t = 30\mu s$ (d) Nozzle N2, $t = 30\mu s$

(e) Nozzle N1, $t = 40\mu s$ (f) Nozzle N2, $t = 40\mu s$

Figure 6. Near-field velocity profiles of sprays generated by nozzles N1 and N2 at 800 bar

Figs. 6 and 7 show the velocity profiles for the nozzles N1 and N2 for different injection pressures. Most of our observations and conclusions about the effects of pressure are also true for the other nozzle. For instance, higher injection pressure increases spray development rate, elevates overall velocity and radially expands the spray. Although spray leading

edge does not show deviation in this case (Nozzle N2), however, we can observe higher velocity on the right side of the leading edge and it is expected slight deviation at a more downstream region, where is not in the field of view. Nozzle N2 has a smaller hole diameter than nozzle N1 and it is expected to observe a greater flow velocities compared to nozzle N1 under the same injection pressure. The presented results in Figs. 6 and 7 confirm this. Moreover, it seems that at 1600 bar, the velocity differences between the nozzles are more significant compared to the other case with 800 bar pressure. In addition to the speed map, we can also realize this from the amount of spray penetration within the same time intervals. As stated earlier, slight increase in injection pressure affects the radial velocity component and causes a small increase in the spray cross-sectional area. However, as Figs. 6 and 7 indicate, the cross-sectional area of the spray for the nozzle N2 is more expanded than nozzle N1. The potential reason could be the difference in k-factor as it has been found that nozzles with smaller k-factor are more prone to cavitate [22]. In addition, some studies confirm that, the cone angle and the cross-sectional area of the spray increase for nozzles with smaller k-factor [4, 23]. We also noticed that the influence of injection pressure on radial spray expansion seems to be very small compared to geometry effects.

Conclusion

This study was an attempt to measure the instantaneous velocity of the near-field spray by means of ballistic imaging and fast normalized cross-corrosion methods. One of the important goals in these experiments was to investigate the effects of pressure and nozzle geometry on the near-field velocity profile and spray development. In this study, we found that increasing the injection pressure speeds up the spray development and makes the transient phase shorter in time. As closer it gets to the developed phase, the velocity field becomes more uniform. We also noticed velocity is quite low within 0.5 mm distance from the nozzle tip. Since the liquid column in the central region is optically dense, it is believed that increasing image resolution will provide more details about this specific region in the future experiments. These experiments also showed that nozzle geometry affects the velocity profile as well as the appearance of the near-field spray; the nozzle with smaller hole diameter generates sprays with higher overall velocity compared to larger hole diameter. In addition, although increasing pressure widens spray, but that is negligible compared to nozzle geometry effect.

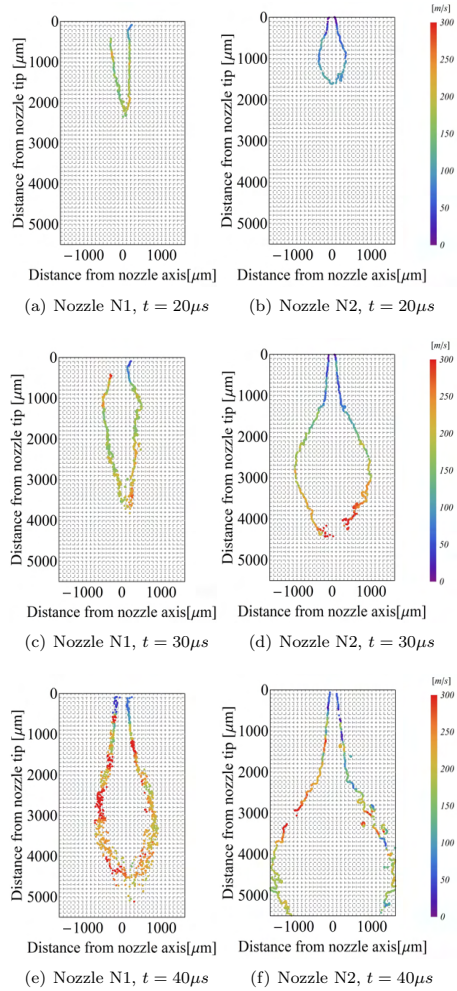

(a) Nozzle N1, $t = 20\mu s$ (b) Nozzle N2, $t = 20\mu s$

(c) Nozzle N1, $t = 30\mu s$ (d) Nozzle N2, $t = 30\mu s$

(e) Nozzle N1, $t = 40\mu s$ (f) Nozzle N2, $t = 40\mu s$

Figure 7. Near-field Velocity profiles of sprays generated by nozzles N1 and N2 at 1600 bar

Acknowledgement

The authors would like to thank Combustion Engine Research Center (CERC), affiliated to Chalmers University of Technology. Special thanks to Dennis Konstanzer and Johan Linderyd.

References

[1] S. Gopinath, P. K. Devan, V. Sabarish, B. V. Sabharish Babu, S. Sakthivel, and P. Vignesh. *Materials Today: Proceedings*, 33, 2020.

[2] J. M. Desantes, J. M. García-Oliver, T. Xuan, and W. Vera-Tudela. *Fuel*, 207:323–335, 2017.

[3] Raul Payri, Juan P. Viera, Venkatesh Gopalakrishnan, and Patrick G. Szymkowicz. *Fuel*, 183, 2016.

[4] Chenglong Tang, Zehao Feng, Cheng Zhan, Wen'an Ma, and Zuohua Huang. *Fuel*, 202:583–594, 2017.

[5] Dong Han, Jiaqi Zhai, Yaozong Duan, Chunhai Wang, and Zhen Huang. *Energy*, 153:223–230, 2018.

[6] Wei Du, Juejue Lou, Yu Yan, Wenhua Bao, and Fushui Liu. *Applied Thermal Engineering*, 121:234–241, 2017.

[7] Meshack Hawi, Hidenori Kosaka, Susumu Sato, Tsuyoshi Nagasawa, Ahmed Elwardany, and Mahmoud Ahmed. *Fuel*, 254:115674, 2019.

[8] Yijie Wei, Tie Li, Xinyi Zhou, and Zhifei Zhang. *Fuel*, 268:117343, 2020.

[9] A. Wierzba. *Experiments in Fluids*, 9(1):59–64, 1990.

[10] José M. Desantes, José V. Pastor, José M. García-Oliver, and Francisco J. Briceño. *Combustion and Flame*, 161(8):2137–2150, 2014.

[11] Johannes Gürtler, Raimund Schlüßler, Andreas Fischer, and Jürgen Czarske. *Optics and Lasers in Engineering*, 90:91–100, 2017.

[12] Z.-M. Cao, K. Nishino, S. Mizuno, and K. Torii. *Experiments in Fluids*, 29(1), 2000.

[13] Raul Payri, Juan P. Viera, Hua Wang, and Louis-Marie Malbec. *International Journal of Multiphase Flow*, 80, 2016.

[14] Zehao Feng, Chenglong Tang, Yue Yin, Peng Zhang, and Zuohua Huang. *International Journal of Heat and Mass Transfer*, 133, 2019.

[15] Raimund Schlüßler, Johannes Gürtler, Jürgen Czarske, and Andreas Fischer. *Experiments in Fluids*, 56(9):176, 2015.

[16] Mark Linne. *Progress in Energy and Combustion Science*, 39(5):403–440, 2013.

[17] Mark A. Linne, Megan Paciaroni, Edouard Berrocal, and David Sedarsky. *Proceedings of the Combustion Institute*, 32(2), 2009.

[18] Harsh Purwar, Saïd Idlahcen, Claude Rozé, David Sedarsky, and Jean-Bernard Blaisot. *Optics Express*, 22(13), 2014.

[19] David Sedarsky, Saïd Idlahcen, Jean-Bernard Blaisot, and Claude Rozé. *Experiments in Fluids*, 54(2):1451, 2013.

[20] Fei Yan, Yuchen Du, Lihui Wang, Wenxian Tang, Jian Zhang, Bo Liu, and Chenpeng Liu. *International Journal of Spray and Combustion Dynamics*, 9(3), 2017.

[21] F. J. Salvador, J. Gimeno, J. De la Morena, and L. A. González-Montero. *Fuel*, 292:120296, 2021.

[22] Anqi Zhang, Alessandro Montanaro, Luigi Allocca, Jeffrey Naber, and Seong-Young Lee. *SAE International Journal of Engines*, 7(2):1034–1043, 2014.

[23] Chengjun Du, Mats Andersson, and Sven Andersson. *SAE International Journal of Fuels and Lubricants*, 9, 2016.

Publication B

Effect of asymmetrical orifice inlet geometry on spray kinematics and development

Highlights

Effect of asymmetrical orifice inlet geometry on spray kinematics and development

Mohammad Nikouei, David Sedarsky

- We have statistically measured the planar velocity of near-field diesel sprays for the on-axis, off-axis, and two-hole nozzle.

  The asymmetrical off-axis orifice creates spray deflection towards the side where the orifice inlet has more sharpness. In addition, the spray velocity profile at two sides of the spray shows asymmetrical velocity distribution.

- Velocity magnitude at the beginning of injection is much higher for the single-hole off-axis nozzle than for the two-hole nozzle. However, this difference becomes less significant when the needle reaches its maximum lift.

- Injection pressure mainly affects spray evolution timing and overall velocity. However, it does not significantly influence the average spray profile.

Effect of asymmetrical orifice inlet geometry on spray kinematics and development

Mohammad Nikouei[a,b], David Sedarsky[a]

[a]*Chalmers University of Technology, Gothenburg, Sweden*
[b]*Scania CV AB, Södertälje, Sweden*

Abstract

In diesel engines, fuel injection has a commanding effect on combustion. Thus studying diesel spray characteristics is beneficial for controlling and improving diesel combustion. However, information on diesel spray characteristics, especially those by injector needle lift, is lacking. This study investigates the near-nozzle spray kinematics for particular nozzle geometries over a range of injection pressures. The nozzles used in this research include a single-hole off-axis nozzle and a two-hole nozzle with deviated orifices. This study aims to observe the effect of asymmetrical orifice inlet on the spray kinematics and describe how sensitive they are to the injection pressure. First, we applied double-pulses time-gated ballistic imaging to obtain well-defined spray/gas interfaces. Then, by tracking these interface structures, we obtained spray kinematics. The results show that the two-hole nozzle generates slower sprays than the single-hole nozzle at the beginning of injection. However, the velocity differences between these sprays become less significant as the sprays develop to a quasi-steady state. In addition, the velocity diagrams show that the instabilities cause the flow to experience significant velocity alterations at the beginning of the injection. Moreover, we observed that the nominal spray axis shift towards the sharper orifice inlet edge, which will affect the spray targeting. Finally, the injection pressure seems to have minimal effect on the spray profile, but it certainly changes spray evolution timing and shortens the transient phase.

Keywords:
Diesel, Spray, Near-field, Nozzle geometry, Ballistic imaging

1. Introduction

In Compression Ignition (CI) engines, fuel injection has a commanding effect on combustion. In other words, controlling injection parameters can influence combus-

tion products. However, this is not simple since the number of parameters affecting fuel spray characteristics is relatively large. In addition, these parameters are not independent. Hence, interactions between injection parameters make it complicated to find the optimum configuration for different work conditions. Some sources address the effect of parameters such as injection pressure [1, 2, 3] and temperature [4] on spray characteristics. In addition, experiments with different fuels show that the fuel properties can also affect spray behavior [2, 5, 6], mainly due to their physical properties, such as viscosity and boiling temperature. Furthermore, studies show that the design of nozzle geometry plays an essential role in spray break-up [6, 7] and even the combustion products [8]. However, the nozzle geometry itself consists of several parameters such as hole diameter, orifice length, orifice angle, edge roundness, and conicity level. Moreover, if the cross-section of the orifice exists in shape other than a circle (e.g., elliptical shape [9]), even more parameters will be involved. Although these geometrical parameters have been studied earlier [10, 11], however, little attention has been paid to the effect of asymmetrical inlet geometries on spray behavior. For this purpose, we have selected two specially built nozzles to investigate the effect of asymmetrical inlet geometries. These asymmetries are usually present in conventional multi-hole injectors used in production. The asymmetry level of the orifice inlet changes by orifice position or its inclination angle. In addition, measurements of penetration length over time [12] show a relation between orifice angle and penetration velocity. Therefore, the study of spray velocity profile in angled orifices would be complementary. Hence, we intend to explain spray behavior by measuring and analyzing near-field spray velocity profile characteristics. According to Zama et al. [13] the spray post-impingement behavior depends on its velocity profile prior to impingement because velocity can influence the heat transfer mechanism. Accordingly, it is possible to predict spray behavior by near-field velocity profile.

Various methods have been used to measure spray velocity for different spray regions and Sedarsky et al.[14] have listed the advantages and disadvantages of some of these methods including LCV, LDV, PIV, and CIV. However, the presence of ultra-dense liquid core in the near-field does not allow the implementation of most of the mentioned techniques, especially the PIV [15]. The PIV method requires tracking particles while no particle can be detected in the near-field, since the dense liquid core obscures them. Hence, we only track the spray interfaces as a solution to measure near-field spray kinematics. This approach requires clear and distinguishable spray structures. In order to obtain well-defined structures, we apply time-gated ballistic imaging [16], which is a line-of-sight imaging method. This imaging setup can reduce multiple-scattering noises and provide a high-resolution spray interface. This method was initially used for medical applications, but it was also used for study spray after

a while.

Similar to Sedarsky et al. [14], we have applied cross-correlation on double-exposure images to measure the gas/liquid interface's velocity. However, in the current work, we have focused on the effect of specific inlet geometries on spray kinematics. In order to measure fluid interface velocity, we need pairs of images to apply correlation and extract displacement vectors. Therefore, we apply two synchronized laser pulses to collect a pair of consecutive images of the same injection event. In Section 2, we have described image acquisition and experimental setup details. Section 2.5 provides data processing and analysis and explains how we extracted velocity data. Finally, Section 3 shows the results and velocity profiles, followed by a discussion about how the spray behavior and velocity profiles affected by inlet geometries and injection pressure.

2. Experimental Setup

2.1. Image acquisition

As mentioned earlier, the main objective of this research is to measure and compare near-field sprays generated by asymmetrical orifice inlet geometries. At a very short distance to the nozzle, no or just a little break-up occurs, and therefore, it is challenging to identify and track seeding particles. On that account, one can suggest tracking fluid interface instead of seeding particles; however, this solution requires high spatial resolution images with well-defined structures. The time-gated ballistic imaging method filters noise from multiple scattering and can produce high-resolution images to identify and accurately trace fluid interface structures. However, the ballistic imaging setup requires high-power ultra-short laser pulses.

For this study, we have used two regenerative amplifiers seeded by a common Ti-Sapphire oscillator. The output beams consist of ultra-short (femtosecond) pulses with the wavelength of 800 nm. Pulse emission frequency is 1 kHz, which is insufficient to capture consecutive images of a whole injection event. Therefore, we use two light sources that are aligned and synchronized together. As Fig. 1 illustrates, laser pulses are divided into two parts using a beam splitter. The first portion is used as the light source for imaging, while the other portion activates birefringence in a carbon disulfide (CS_2) cell. We have evaluated activation period for CS_2 to be slightly less than 2 ps. During this period, the polarization of transmitted photons rotates by 90°. We place the CS_2 cell between two polarizers, perpendicular to each other. With this configuration, the photons passing through the first polarizer can only pass through the second polarizer when the CS_2's birefringence is active. This configuration allows only the photons with the least interaction with spray to reach

the detector and filter the rest of the multiple scattering photons. When the imaging beam is transmitted through a Barium Borate (BBO) Crystal, its frequency is doubled, minimizing the interaction between the imaging and switching beam. This configuration is known as co-linear ballistic imaging [17].

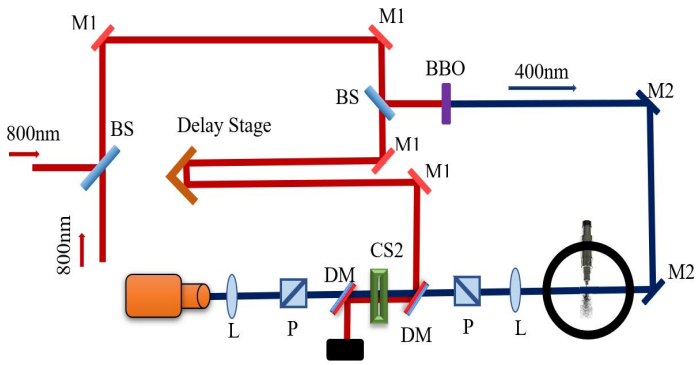

Figur 1: A schematic view of image acquisition system configuration. M1: 800 nm mirror, M2: 400 nm mirror, BS: beam splitter, P: polarizer, L: lens, DM: dichroich mirror.

We have used an ICCD camera (PI-Max 4) for capturing images. The dwell time between each shot should be set as short as possible to retain the spray structure, but it should also be long enough to allow the sensor phosphor to decay. The trade-off between these requirements showed that 560 ns is suitable for this application. The resolution of the camera sensor is 1024 $\times$ 1024 pixels, and the spatial resolution of the optical setup is measured to be 8.33 μm per pixel length.

2.2. Hardware

The injectors used in this study are the XPI (eXtra high-Pressure Injector), designed and developed by Cummins. These injectors are side-fed, and due to the geometrical constraints, there is no choice but to install the injector diagonally on the chamber. In this setup, the angle between the injector and the horizontal axis is 21°. We perform experiments on three prototype nozzles with different geometries to study the effect of inlet geometry on near-field spray velocity. As it illustrated in Fig. 2, one of the nozzles is a normal single-hole nozzle and its orifice axis is located in the middle of the sac. The second nozzle is also a single-hole but with an off-axis orifice.

Tabell 1: Nozzles specifications

Nozzle	SH	OA	$TH-A$	$TH-B$
Outlet diameter [μm]	178	224	205	200
Inlet diameter [μm]	198	234	224	219
Orifice Length [mm]	1	0.7	1	1
k-factor	2	1.4	2	2
Hydro-grinding level [%]	30	15	15	15

Finally the last one is a two-hole nozzle with deviated orifices in which their umbrella angle is 146°. Fig 2 illustrates the schematic half section view of these nozzles. This Figure shows how the curvature of the sac volume and the position of orifices can create asymmetrical geometry at the orifice inlet and outlet. Therefore, it is evident that conditions would be different for the flow reaching either side of the orifices in the latter two cases. Table 1 indicates specifications for each orifices; To distinguish the orifices of the two-hole nozzle, we label them with letters A and B. In addition, we use SH, OA and TH abbreviations for referring to the single-hole on-axis, off-axis and the two-hole nozzles, respectively.

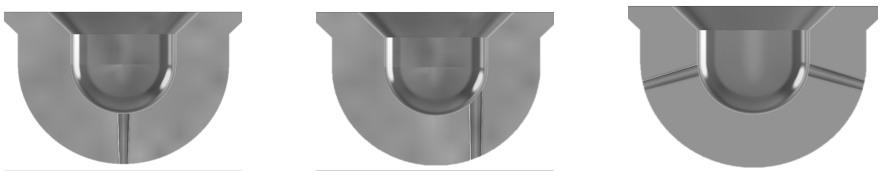

(a) single-hole, on-axis (b) single-hole, off-axis (c) two-hole

Figur 2: Schematic view of nozzle geometry

2.3. Experimental conditions

A high-pressure fuel pump continuously supplies commercially available diesel fuel to the injector over a range of pressures. This pump is equipped with a heat exchanger to cool the fuel with open-loop tap water and keep the fuel temperature constant. We performed experiments with 800, 1200, and 1600 bar of rail pressure in this work. Table 2 shows the other details about the experimental conditions.

Tabell 2: Experimental conditions

Parameter	**Value**	**Unit**
Rail pressure	800, 1200, 1600	bar
Back pressure	atm	-
Ambient temperature	294	K
Injection duration	2	ms

2.4. Experiment procedure

We set the injector triggering signal to 2 ms. Since laser pulses frequency is 1 kHz (one pulse per millisecond), we cannot take more than a pair of images per injection event. Therefore, we estimate velocities based on a statistical average of several injection events to cope with this limitation. For this purpose, we took at least 150 image pairs for each discreet time instants after the start of injection. Studies include time instants from 20 to 50 μs after Hydraulic Start Of Injection (HSOI) with increments of 10 μs. HSOI is the reference time and it is unique for each orifice. HOSI is described as the moment when the fuel is on the verge of leaving the nozzle. In order to get this time instant, we take a bunch of images with 1 μs of intervals just before emergence of fuel until it comes out of the nozzle. At the initial stage of spray penetration, spray penetration grows linearly with the time because the momentum exchange rate between the liquid column and surrounding air is close to zero [18]. Therefore, during the very early stage of injection, the velocity of spray penetration is calculated based on spray penetration length. Accordingly, the relative timing for penetration equal to zero is obtained, and we set other time intervals according to this point.

2.5. Data processing

All images undergo normalization and background subtraction. Next, we rotate images to align the orifice axis with the vertical axis for all cases. In some cases, we also flipped images horizontally so that the sharper edge of the orifice lays on the left side of the vertical axis. Performing a fast normalized cross-correlation on image pairs provides displacement vectors across the spray periphery. For this purpose, the spray edge is detected first by the Sobel algorithm. Then, we randomly distribute several target points on the spray edge (Fig. 3). The information around each target point, including the pattern and intensity, is captured in the next step. This information is correlated within a certain distance from the same coordinates on the second image. Finally, all correlations undergo a validation test, which is done based on the

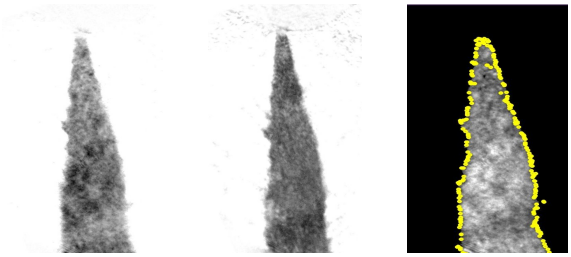

(a) t_1 (b) $t_1 + 560ns$ (c) Target points

Figur 3: Example of one image pair taken with a time difference of 560 ns and distribution of target points

correlation coefficient or the percentage of similarity and the maximum and minimum anticipated values for displacement. Fig. 4 visually explains this process, that yields displacement vectors of the spray periphery on a 2D plane over a specific time. In the last step, we calculate the velocity magnitude of each point assuming that the displacement in the direction normal to the plane is equal to the displacement in the horizontal direction.

Since there are shot-to-shot variations in spray profile, therefore, we extract velocity data for Average Spray Profile (ASP) at each time instant and injection pressure. For each coordinate on the ASP (Fig. 5(a)), mean velocity is calculated by averaging the velocity data available in the vicinity (8×8 pixels) of the respective point. The source of this velocity data is velocity vectors extracted from all individual image pairs at respective time instant and injection pressure (Fig. 5(b)).

3. Results and Discussion

The main results of the experiments are statistical velocity maps of the near-field spray periphery. We have combined these velocity maps in Figs. 6, 7 and 8. In these images, each column represents the time instant after HSOI, and each row belongs to a particular injection pressure. In each plot, a set of points indicate the approximate spray interface at the corresponding time instant. The vertical and horizontal axes show the coordinates of each point relative to the nozzle tip, and the color of each point indicates the average spray velocity magnitude around that point.It should be noted that in the image processing stage, we have rotated or flipped all the images so that all orifice axes coincides with the vertical axis and the sharper edge of the orifice inlet has been placed on the left side.

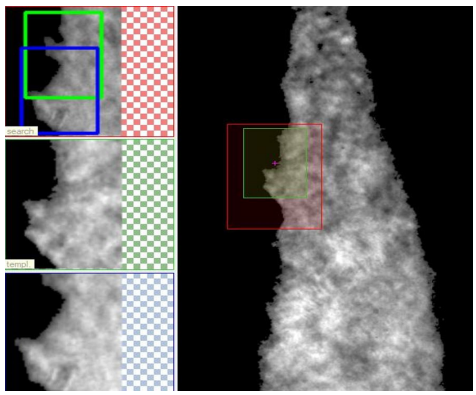

Figur 4: An example of spray tracking. On the left side, green square shows the position of the template in the first image and the blue square is the matched template from the second image. The red box indicates the search field.

These images show that the velocity magnitudes of TH nozzle's sprays are considerably lower than for the OA. According to continuity in fluids, the increase in cross-sectional area under constant pressure is inversely proportional to the velocity of the fluid; therefore, it seems that the larger total cross-sectional area at the TH nozzle outlet lowers the velocity in both TH nozzle's orifices. However, the difference between velocity magnitudes becomes less significant at the quasi-steady state (800 μs). Therefore, the position of the injector needle seems to be important in this case. We assume that the needle is still at a low lift at the beginning of the injection, which delivers a very low incoming flow rate to the sac volume. On the other hand, the total cross-sectional area of TH nozzle is larger than the OA. Therefore, it will take longer for the TH nozzle to recover its sac pressure.

Unlike other nozzles, the spray of the SH nozzle is formed at a slower speed and is narrower in its shape. In this nozzle, there is no change in the direction of the internal flow as severely as in the other nozzles since there is no orifice inclination nor the asymmetry that exists in the OA nozzle. These two critical factors, and possibly the smaller diameter of the orifice, cause significant differences in spray behavior and velocity distribution for SH nozzle. Fig. 9 and 10 display the average radial and axial velocity distribution for the SH nozzle, respectively. These diagrams shows that the spray initially has a low axial velocity. However, the axial velocity gradually increases over time from the start of the injection. Radial velocities are very close to zero, which indicates a minimal amount of expansion in the radial direction of

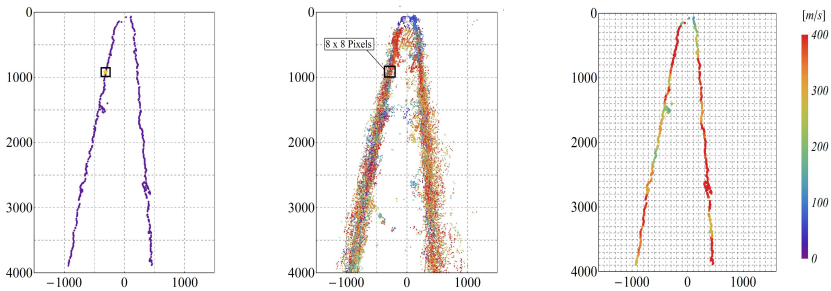

(a) (b) (c)

Figur 5: Example of one image pair taken with a time difference of 560 ns and distribution of target points. a)Target point representing average spray profile, b) all measured velocity data, c)average velocity profile on average spray profile

the spray. As stated earlier, we hypothesized the possible reason for the lower spray velocities in the TH nozzle, which is the larger cross-sectional area. Accordingly, we expected to see higher axial velocities in the spray of the SH nozzle. However, despite the smaller diameter of the SH orifice, the axial velocities of the spray are less than for the OA's. Analyses show that the SH nozzle's spray penetration is approximately equal to that of the OA. Thus, this indicates that the velocity of the liquid core is equal to or greater than the OA's spray centerline. Nevertheless, there seems to be more friction around the SH's orifice wall, which dissipates the flow energy on the spray periphery.

The results show that the velocity is very low in the region close to the nozzle outlet, especially at the beginning of the injection. The flow accelerates within a short time after the start of injection and reaches a maximum relative value when it goes to the quasi-steady state (800 μs). Therefore, it is supposed that the initial velocity of the primary fuel portion that leaves the nozzle is close to zero. However, The velocity at the orifice exit increases over time. As time goes on, the needle lift increases and causes higher flow acceleration inside the injector cavity. Therefore, the fluid velocity exceeds the initial value when departing the nozzle at later time instants. It should be noted that this acceleration does not continue uniformly, and we have observed slight deceleration in the middle of the early transient phase. At the beginning of the injection, the spray tip velocity is higher than its upstream flow. Accordingly, it is supposed that the flow starts accelerating after leaving the nozzle. However, as mentioned earlier, the upstream flow accelerates shortly afterward. In addition,

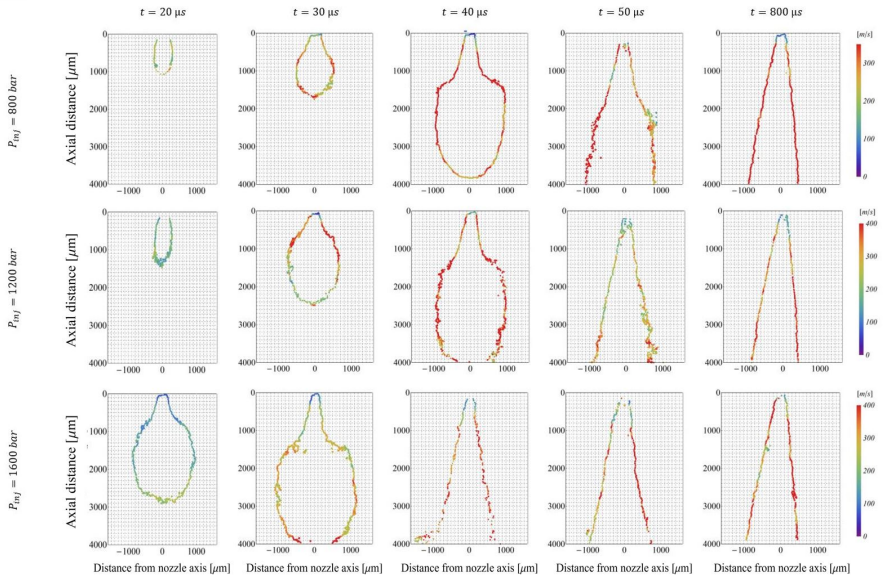

Figur 6: Mean velocity magnitude for the off-axis nozzle over a range of pressures and timings

the leading edge slows down, which can have various reasons, such as induced drag force or the rise of instabilities. In addition, Tang et al. have also noticed a slight deceleration in spray tip penetration which they believe is caused by break-up of a mushroom shaped mass fraction [11]. Similarly, we can observe such a shape in the spray evolution pattern at the beginning of injection. As Crua et al. have identified [19], perhaps this fraction is a mixture of residual liquid fuel and gas trapped in the sac volume between the injections.

It seems that velocity differential at upstream and downstream could also contribute in forming the mushroom-shaped mass at the beginning of the injection. This mass forms and grows near the nozzle and travels downstream. The amount of surface expansion of this mass depends on the geometry of the nozzle, but the results show that it is not very sensitive to the injection pressure. Comparison of spray profiles shows that the extent of this mass is the greatest in the OA nozzle, and the SH nozzle creates the least expansion. In addition, the growth rate of this mass is almost at the same level in both orifices of the TH nozzle. According to the

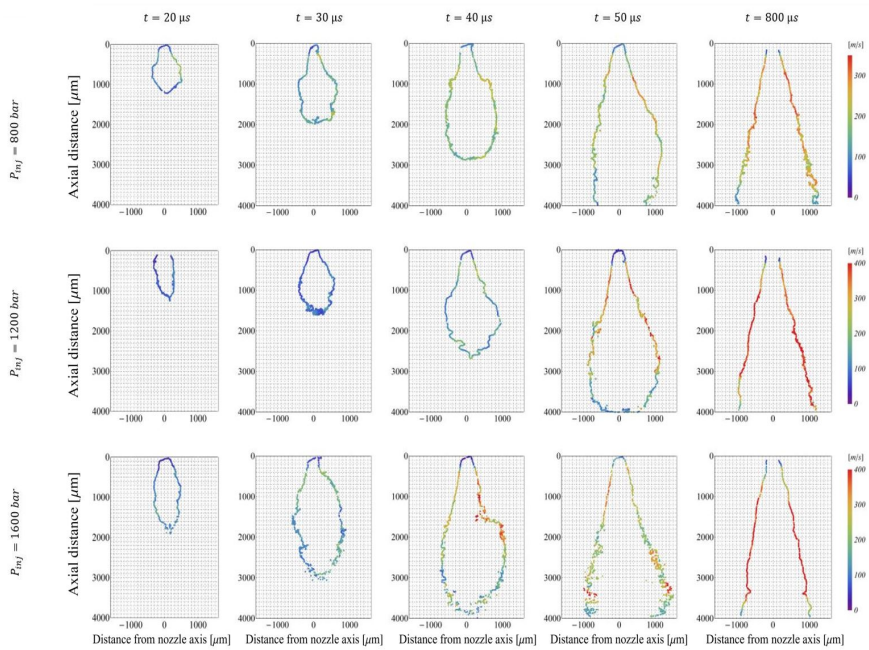

Figur 7: Mean velocity magnitude for the TH-A orifice over a range of pressures and timings

geometry of these nozzles, it is presumed that they are mainly different potentials for generating cavitation. In addition, the internal flow streamline of each nozzle is distinct. However, since cavitation is associated with the injection pressure, thus cavitation can not be the main reason for the formation of this mushroom-shaped mass; otherwise, the size of this mass should have changed significantly by increasing the injection pressure. Therefore, to find the root cause of the formation of this mass and the factors affecting it, we must pay attention to other factors, including the internal flow streamline.

According to Figs. 7 and 8, the formation of this mass is similar in both TH orifices but slightly different than other nozzles. For these orifices, an arc is formed on the right side of the spray. Inspection of orifice walls on the left and right sides of the spray shows that the flow on the right side exits slightly earlier than on the other side; the spherical outer surface of the nozzle created uneven orifice walls so

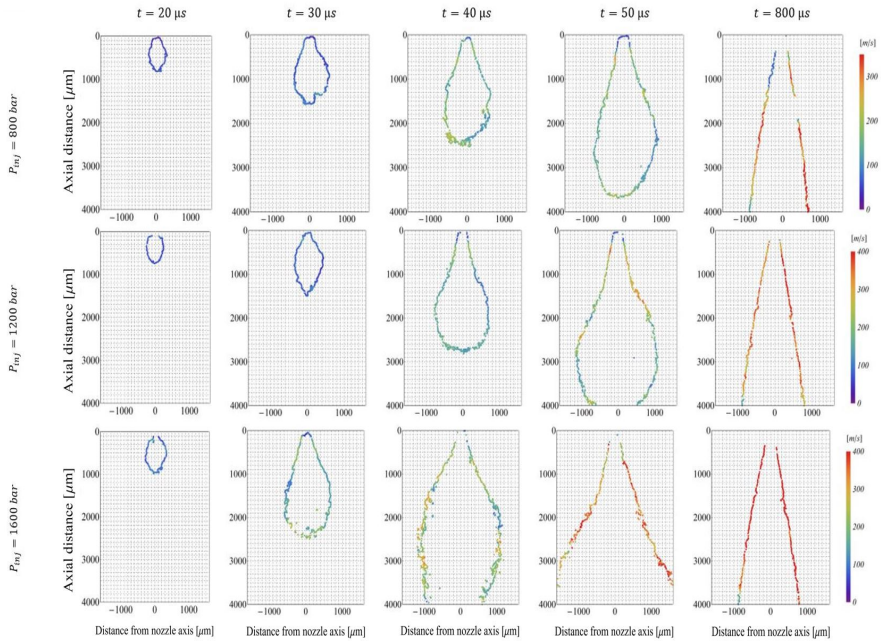

Figur 8: Mean velocity magnitude for the TH-A orifice over a range of pressures and timings

that the right wall is shorter than the left one. In addition, at the orifice inlet, the left edge looks sharper. However, neither of these two points can explain such spray behavior reasonably because these features are also present in the OA nozzle, while no asymmetrical arc forms within the spray of this nozzle. Nevertheless, the main difference between the OA and TH nozzles is the inclination of the orifices from the injector axis. This inclination appears to create momentum in the flow, which leads to forming an arc on the right side of the spray. In both cases, the arc is formed on the lower wall, making this conclusion more sensible.

As mentioned earlier, the extent of the mushroom-shaped mass in the OA nozzle is the highest and formed differently from the other two nozzles. Analysis of velocity components in the radial direction expresses an outstanding behavior. As Fig. 11 shows, at the beginning of injection, the radial velocities on the right side of the spray are pointing towards positive values of the transverse axis, while on the other side

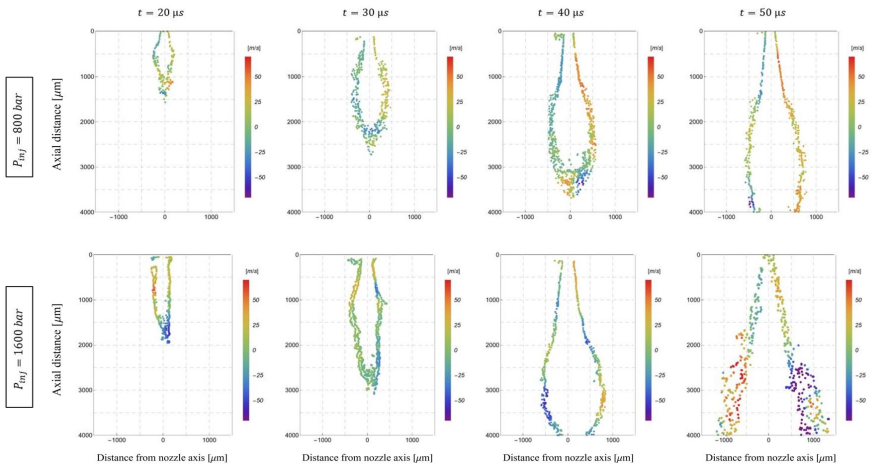

Figur 9: Radial velocity distribution for single hole, on-axis orifice over two different injection pressures

velocities are negative, meaning that the mushroom-shaped mass volume expands to the sides. However, an interesting point arises in later time instants: at 30 and 40μs radial velocity components at the top of this mass have an inverted direction while the bottom of this mass keeps the same radial velocity direction as at the beginning of injection. This process is independent of injection pressure, and according to Fig. 11, such a case is observable in all studied injection pressures. This result suggests that vortices are likely to form inside the mass fraction, creating a tumble that is reflected in the radial velocity profile. Assuming that the accelerating flow in the center of the spray penetrates into this mass at high relative velocity, it probably creates a relative vacuum inside the mass upstream which can be explained graphically by Fig. 12. However, the axial velocity of the liquid core and the mass downstream get synchronized. It is thought that this mechanism improve the air entrainment, but on the other hand, it induces a loss in the axial flow and impedes acceleration in the axial direction.

Studying the TH nozzle and its spray velocity distribution diagrams can provide information regarding hole-to-hole variation and interaction. In addition, that will help investigate the effect of orifice inclination. Analysis of eccentric needle movement addresses that sprays of a multi-hole injector are not identical, while their axial

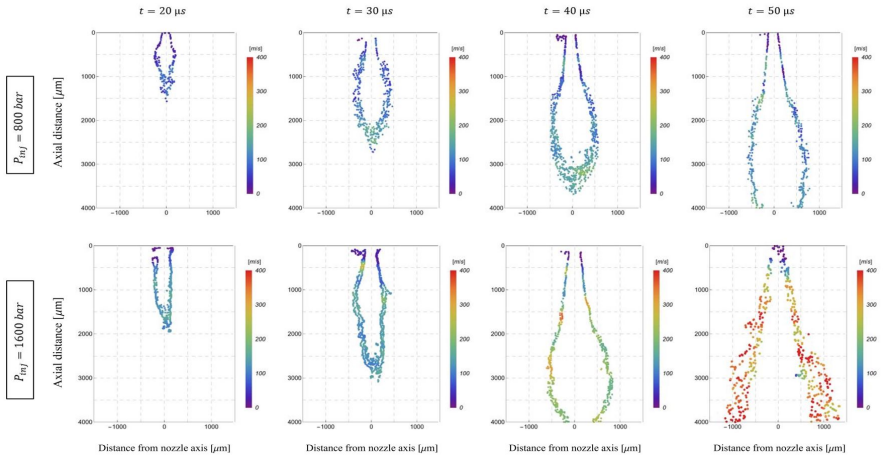

Figur 10: Axial velocity distribution for single hole, on-axis orifice over two different injection pressures

velocities fluctuate over the injection period. In other words, the dynamics of each spray fluctuate under a particular frequency, and that frequency is independent of injection pressure, and the number of holes [20]. According to this study, the primary cause of this fluctuation is the eccentric movement of the needle. In addition, since there is no phase lag in axial velocity oscillation, thus the variation in sac pressure is the main contributor to that matter rather than hole-to-hole variation. In the current study, since the TH nozzle has only two holes, the sac pressure variation is expected to be less than the conventional injectors with nozzles of 8 to 12 holes. This study shows that the sprays of TH-A and TH-B undergo their unique evolutionary path, although both orifices have a similar rate of development. However, the radial velocities are higher in TH-B, which has led to a more significant radial expansion during the early transient phase as it is evident in Fig. 13. This behavior could be primarily due to the minor geometrical differences between orifices.

Moreover, due to the geometrical constraints of the chamber and injector fuel line, we had to mount the injector body diagonally. The angle between the injector axis and horizontal plane in this configuration becomes 21°. Consequently, the angle between the vertical axis and TH-A orifice will be 4° while this value is equal to 142° for the case of TH-B. Therefore, the fluid inside the nozzle experiences a more

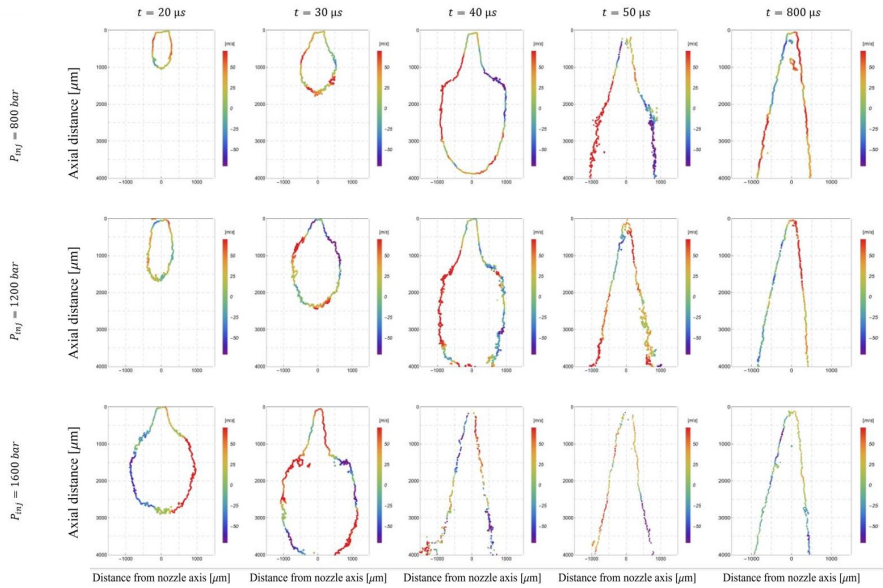

Figur 11: Radial velocity distribution for the off-axis nozzle over a range of pressures and timings

severe change in its direction to exit TH-B. This rotation in the flow direction induces centrifugal and centripetal forces on the spray periphery, which results in more spray expansion. In addition, with higher injection pressures, radial velocities also increase in both TH-A and TH-B orifices. It is evident by comparing sprays of TH-A and TH-B at 50 microseconds at every injection pressure.

Another point worth noting is the differences in average penetration and overall velocities in TH-A and TH-B cases. Comparing these sprays within the same time frame and pressure indicates that TH-B's overall velocity magnitude is slightly smaller at every injection pressure. A potential reason could be related to the installation angle of the injector body. As mentioned earlier, the internal flow is likely to experience more bends, which induces a loss in the flow. Therefore, we suspect that the injector orientation might contribute to hole-to-hole spray variation in multi-hole injectors. Hence, the installation angle is likely to influence the internal flow and the near-field spray velocity. We can easily verify this hypothesis in the future by rotating the injector by 180° and exchanging the position of each orifice. However,

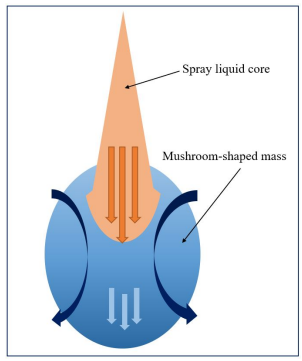

Figur 12: A graphical representation of the hypothesis of induced Tumble in the mushroom-shaped mass by the spray liquid core.

the minor geometrical differences between these orifices might also contribute to this matter.

Spray profiles in Figs. 6,7 and 8 show another debatable issue; after 40 or 50 μs, the left side of the spray inclines toward the negative side of the horizontal axis. In addition, the right side of the spray also tends to incline toward the left side and forms a small arc on the right side of the spray. Deviation toward the left side is even more evident in the quasi-steady state. Although this is not the case in orifice TH-A, it is visible in the other two orifices (OA and TH-B), regardless of injection pressure. In addition, the velocity profiles at 800 μs, indicate that the velocity magnitudes on the left side of the spray are lower than on the right side. It becomes more interesting when we realize that sharper orifice inlet edge is also located at the left side. Increasing the pressure seems to exacerbate this velocity asymmetry. Therefore, we expect that the increase in injection pressure boosts the deviation angle, although this change seems negligible according to the results. However, to find a more accurate answer in this regard, investigation in the far-field might be required.

Investigations of the effect of injection pressure show that the injection pressure directly influences the timing of spray evolution because it reduces the nozzle opening and closing delay and consequently shortens the transient phases. In addition, the maximum relative velocity goes higher with raising the injection pressure. However, regarding the physical characteristics, the effect of pressure on the average spray profile is negligible at the quasi-steady state. We also observed a similar spray evolution pattern in the early transient phase; however, these similar patterns appear at ear-

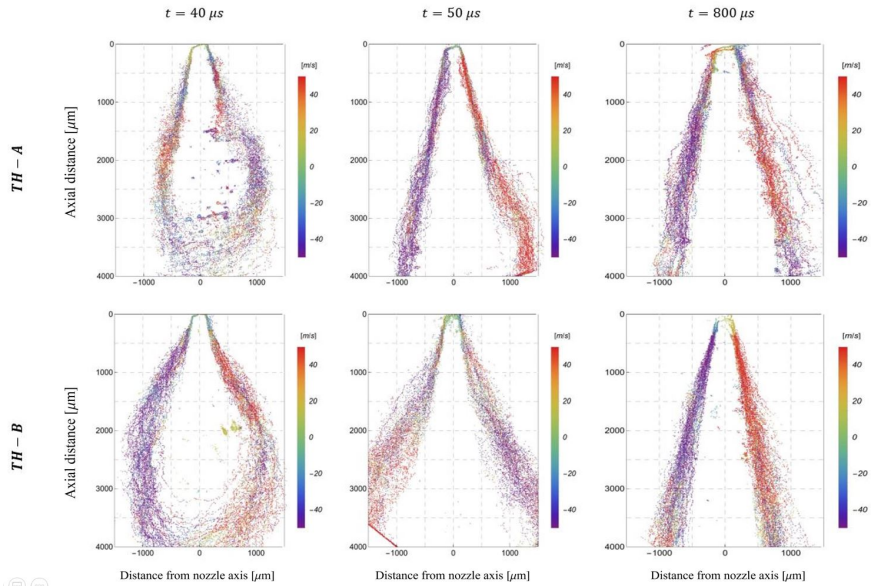

Figur 13: Radial velocity distribution for the two-hole nozzle over a range of timings at 1600 bar injection pressure.

lier time stages when pressure is higher. To clarify this statement, we can compare average spray profile at 30 μs & 1600 bar with the one at 40 μs & 800 or 40 μs & 1200 bar. Nevertheless, overall velocity magnitudes are much different in these cases. In other words, comparing two cases with the same penetration length but different injection pressure, the velocity is higher in the case with higher pressure. Therefore, higher injection pressure raises the spray acceleration in the early transient phase. On the other hand, the nozzle opening delay becomes smaller with pressure rise, indicating a higher acceleration of needle motion. Therefore, one can conclude that the spray acceleration is primarily a function of the needle acceleration in the transient phase. However, the overall force acting on the needle is proportional to the injection pressure, and thus increasing the injection pressure transforms into a higher acceleration in the needle.

The analysis of the effect of injection pressure on TH-A and TH-B shows a surprising point. As Figs. 7 and 8 depict, velocities and penetration at 1200 bar are unexpectedly lower or relatively equal to the 800 bar condition. This effect is less

likely to result from error or accident because we performed the image acquisition for each time instant/pressure over different days with the same setup. Nevertheless, by increasing the injection pressure to 1600 bar, the flow accelerates and penetration at respective time instants improves. Perhaps in near-field spray evolution, there might be a critical injection pressure so that the turbulent interactions and instabilities suppress the growth in spray velocity. However, elevating the injection pressure beyond that critical value would overcome the losses induced. By the way, to justify this hypothesis, we need more statistics. In addition, the nozzles' internal flow characteristics can also provide a window to the correct answer.

4. Conclusion

This study visualized the kinematics of near-field diesel spray for asymmetrical nozzle geometries. In this study, we measured and collected velocity information for 45 sprays in total, which belong to 3 orifices, three injection pressures, and five time-instants. In addition, more than 150 image pairs were taken and processed for each of these sprays to statistically investigate the effect of asymmetrical orifice inlet on the spray kinematics.

The results show that the near-field spray velocity for the single-hole off-axis nozzle is higher than those sprays generated by the two-hole nozzle at the beginning of injection. This difference could be the consequence of different outlet cross-sectional areas. However, as the needle lift increases and the flow reaches a quasi-steady state, they show less significant velocity differences. We observed that generally, the flow starts accelerating upon exiting the orifice. In addition, the velocity diagrams show that near-field velocity alternates at the beginning of injection, which could be due to the flow instabilities. The diagrams also show that the average spray axis deviates from the center towards the side with a sharper orifice inlet edge. This phenomenon is more remarkable for the off-axis nozzle, and it will affect spray targeting. In addition, measurements show that the velocity distribution is not symmetrical on the two sides of the spray when the spray deviates. Finally, the injection pressure mainly impacts nozzle opening delay and can increase the needle acceleration, directly affecting spray acceleration and evolution. Therefore, higher injection pressure reduces the time for spray evolution by increasing the velocity and acceleration of the flow and shortens the transient phase by accelerating the needle movement.

5. Acknowledgments

The authors would like to thank Combustion Engine Research Center (CERC) and the Swedish Energy Agency for funding. Thanks to Dennis Konstanzer and

Johan Linderyd for their support and cooperation.

Referenser

[1] W. Du, J. Lou, Y. Yan, W. Bao, F. Liu, Effects of injection pressure on diesel sprays in constant injection mass condition 121 234–241. doi:10.1016/j.applthermaleng.2017.04.075.
URL https://www.sciencedirect.com/science/article/pii/S1359431116340686

[2] M. Hawi, H. Kosaka, S. Sato, T. Nagasawa, A. Elwardany, M. Ahmed, Effect of injection pressure and ambient density on spray characteristics of diesel and biodiesel surrogate fuels 254 115674. doi:10.1016/j.fuel.2019.115674.
URL https://www.sciencedirect.com/science/article/pii/S0016236119310269

[3] F. J. Salvador, J. Gimeno, J. De la Morena, L. A. González-Montero, Experimental analysis of the injection pressure effect on the near-field structure of liquid fuel sprays 292 120296. doi:10.1016/j.fuel.2021.120296.
URL https://www.sciencedirect.com/science/article/pii/S0016236121001721

[4] Z. Wang, C. Jiang, H. Xu, M. L. Wyszynski, Macroscopic and microscopic characterization of diesel spray under room temperature and low temperature with split injection 142 71–85. doi:10.1016/j.fuproc.2015.10.007.
URL http://www.sciencedirect.com/science/article/pii/S0378382015301946

[5] J. M. Desantes, J. M. García-Oliver, T. Xuan, W. Vera-Tudela, A study on tip penetration velocity and radial expansion of reacting diesel sprays with different fuels 207 323–335. doi:10.1016/j.fuel.2017.06.108.
URL https://www.sciencedirect.com/science/article/pii/S0016236117308177

[6] R. Payri, J. P. Viera, V. Gopalakrishnan, P. G. Szymkowicz, The effect of nozzle geometry over internal flow and spray formation for three different fuels 183 20–33. doi:10.1016/j.fuel.2016.06.041.
URL https://www.sciencedirect.com/science/article/pii/S0016236116304938

[7] C. Du, M. Andersson, S. Andersson, Effects of nozzle geometry on the characteristics of an evaporating diesel spray 9 (3) 493–513. doi:10.4271/2016-01-2197.
URL https://www.sae.org/publications/technical-papers/content/2016-01-2197/?PC=DI

[8] C. Yao, P. Geng, Z. Yin, J. Hu, D. Chen, Y. Ju, Impacts of nozzle geometry on spray combustion of high pressure common rail injectors in a constant volume

combustion chamber 179 235–245. doi:10.1016/j.fuel.2016.03.097.
URL https://www.sciencedirect.com/science/article/pii/S0016236116301399

[9] S. Yu, B. Yin, W. Deng, H. Jia, Z. Ye, B. Xu, H. Xu, Experimental study on the spray characteristics discharging from elliptical diesel nozzle at typical diesel engine conditions 221 28–34. doi:10.1016/j.fuel.2018.02.090.
URL https://www.sciencedirect.com/science/article/pii/S0016236118302497

[10] F. J. Salvador, M. Carreres, D. Jaramillo, J. Martínez-López, Analysis of the combined effect of hydrogrinding process and inclination angle on hydraulic performance of diesel injection nozzles 105 1352–1365. doi:10.1016/j.enconman.2015.08.035.
URL https://www.sciencedirect.com/science/article/pii/S0196890415007815

[11] C. Tang, Z. Feng, C. Zhan, W. Ma, Z. Huang, Experimental study on the effect of injector nozzle k factor on the spray characteristics in a constant volume chamber: Near nozzle spray initiation, the macroscopic and the droplet statistics 202 583–594. doi:10.1016/j.fuel.2017.04.078.
URL https://www.sciencedirect.com/science/article/pii/S0016236117305033

[12] R. Payri, F. J. Salvador, J. De la Morena, V. Pagano, Experimental investigation of the effect of orifices inclination angle in multihole diesel injector nozzles. part 2 – spray characteristics 213 215–221. doi:10.1016/j.fuel.2017.07.076.
URL https://www.sciencedirect.com/science/article/pii/S0016236117309389

[13] Y. Zama, Y. Odawara, T. Furuhata, Experimental investigation on velocity inside a diesel spray after impingement on a wall 203 757–763. doi:10.1016/j.fuel.2017.04.099.
URL https://www.sciencedirect.com/science/article/pii/S0016236117305252

[14] D. Sedarsky, S. Idlahcen, J.-B. Blaisot, C. Rozé, Velocity measurements in the near field of a diesel fuel injector by ultrafast imagery 54 (2) 1451. arXiv:1301.6593, doi:10.1007/s00348-012-1451-9.
URL http://arxiv.org/abs/1301.6593

[15] Z.-M. Cao, K. Nishino, S. Mizuno, K. Torii, PIV measurement of internal structure of diesel fuel spray 29 S211–S219. doi:10.1007/s003480070023.

[16] M. A. Linne, M. Paciaroni, E. Berrocal, D. Sedarsky, Ballistic imaging of liquid breakup processes in dense sprays 32 (2) 2147–2161.

doi:10.1016/j.proci.2008.07.040.
URL https://www.sciencedirect.com/science/article/pii/S1540748908000308

[17] H. Purwar, S. Idlahcen, C. Rozé, D. Sedarsky, J.-B. Blaisot, Collinear, two-color optical kerr effect shutter for ultrafast time-resolved imaging 22 (13) 15778. arXiv:1502.03350, doi:10.1364/OE.22.015778.
URL http://arxiv.org/abs/1502.03350

[18] F. Yan, Y. Du, L. Wang, W. Tang, J. Zhang, B. Liu, C. Liu, Effects of injection pressure on cavitation and spray in marine diesel engine 9 (3) 186–198. doi:10.1177/1756827716672472.
URL https://doi.org/10.1177/1756827716672472

[19] C. Crua, M. R. Heikal, M. R. Gold, Microscopic imaging of the initial stage of diesel spray formation 157 140–150. doi:10.1016/j.fuel.2015.04.041.
URL https://www.sciencedirect.com/science/article/pii/S0016236115004391

[20] W. Huang, S. Moon, Y. Gao, Z. Li, J. Wang, Eccentric needle motion effect on near-nozzle dynamics of diesel spray 206 409–419. doi:10.1016/j.fuel.2017.06.012.
URL http://www.sciencedirect.com/science/article/pii/S0016236117307032